Research article

How many sirtuin genes are out there? evolution of sirtuin genes in vertebrates with a description of a new family member

Juan C. Opazo[1,2,3], Michael W. Vandewege[4], Federico G. Hoffmann[5,6], Kattina Zavala[2], Catalina Meléndez[7], Charlotte Luchsinger[8], Viviana A. Cavieres[7], Luis Vargas-Chacoff[1,9,10,11], Francisco J. Morera[1,12], Patricia V. Burgos[7,13,14], Cheril Tapia-Rojas[7,13], Gonzalo A. Mardones[1,8,15]

[1]Integrative Biology Group, Universidad Austral de Chile, Valdivia, Chile.
[2]Instituto de Ciencias Ambientales y Evolutivas, Facultad de Ciencias, Universidad Austral de Chile, Valdivia, Chile.
[3]Millennium Nucleus of Ion Channel-Associated Diseases (MiNICAD), Valdivia, Chile.
[4]Department of Biology, Eastern New Mexico University, Portales, New Mexico, USA.
[5]Department of Biochemistry, Molecular Biology, Entomology, and Plant Pathology, Mississippi State University, Starkville, Mississippi, USA.
[6]Institute for Genomics, Biocomputing and Biotechnology, Mississippi State University, Starkville, Mississippi, USA.
[7]Centro de Biología Celular y Biomedicina (CEBICEM), Facultad de Medicina y Ciencia, Universidad San Sebastián, Santiago, Chile.
[8]Department of Physiology, School of Medicine, Universidad Austral de Chile, Valdivia, Chile.
[9]Instituto de Ciencias Marinas y Limnológicas, Universidad Austral de Chile, Valdivia, Chile.
[10]Centro Fondap de Investigación de Altas Latitudes (IDEAL), Universidad Austral de Chile, Valdivia, Chile.
[11]Millennium Institute Biodiversity of Antarctic and Subantarctic Ecosystems, BASE, Universidad Austral de Chile, Valdivia, Chile.
[12]Applied Biochemistry Laboratory, Facultad de Ciencias Veterinarias, Instituto de Farmacología y Morfofisiología, Universidad Austral de Chile, Valdivia, Chile.
[13]Centro Ciencia & Vida, Fundación Ciencia & Vida, Santiago, Chile.
[14]Centro de Envejecimiento y Regeneración (CARE-UC), Facultad de Ciencias Biológicas, Pontificia Universidad Católica, Santiago, Chile.
[15]Center for Interdisciplinary Studies of the Nervous System (CISNe), Universidad Austral de Chile, Valdivia, Chile.

Corresponding authors:
Juan C. Opazo, jopazo@gmail.com
Gonzalo A. Mardones, gonzalo.mardones@uach.cl

Abstract

Studying the evolutionary history of gene families is a challenging and exciting task with a wide range of implications. In addition to exploring fundamental questions about the origin and evolution of genes, disentangling their evolution is also critical to those who do functional/structural studies to allow a deeper and more precise interpretation of their results in an evolutionary context. The sirtuin gene family is a group of genes that are involved in a variety of biological functions mostly related to aging. Their duplicative history is an open question, as well as the definition of the repertoire of sirtuin genes among vertebrates. Our results show a well-resolved phylogeny that represents an improvement in our understanding of the duplicative history of the sirtuin gene family. We identified a new sirtuin gene family member (*SIRT8*) that was apparently lost in the last common ancestor of amniotes, but retained in all other groups of jawed vertebrates. According to our experimental analyses, elephant shark SIRT8 protein is located in mitochondria, the overexpression of which leads to an increase in cellular levels of ATP. Moreover, *in vitro* analysis demonstrated it has deacetylase activity being modulated in a similar way to mammalian SIRT3. Our results indicate that there are at least eight sirtuin paralogs among vertebrates and that all of them can be traced back to the last common ancestor of the group that existed between 676 and 615 millions of years ago.

Keywords: aging, deacetylase, gene family evolution, gene duplication, mitochondria, SIRT.

Introduction

The availability of whole-genome sequences in species of all main groups of vertebrates represents an opportunity to unravel the evolution of gene families. The number of genomes and their phylogenetic representativeness in the vertebrate tree of life allows performing robust inferences regarding how gene family members are related to each other and their modes of evolution (Nei and Rooney 2005). The available genomes also open an opportunity to discover new gene lineages that are not currently described maybe because they are not present in model species and/or to the absence of appropriate evolutionary analyses (Wichmann et al. 2016; Céspedes et al. 2017; Himmel et al. 2020). Gene copy number variation could be seen as a natural experiment (Albertson et al. 2009) that could help understand the evolutionary fate of duplicated genes, as individuals with different repertoires can, in principle, fulfill the biological functions with a different combination of paralogs (Gitelman 2007).

The sirtuin gene family, class III of histone deacetylase enzymes (HDACs), is a group of genes that, in mammals, is composed of seven paralogs (*SIRT1-7*) grouped into four classes (Fig. 1)(Frye 2000; Frye 2006). Sirtuin genes are involved in a variety of biological functions mostly related to aging, metabolic regulation, stress response, cell cycle among others (Fig. 1) (Michan and Sinclair 2007; Greiss and Gartner 2009; Haigis and Sinclair 2010; Zhao et al. 2019; Zhang et al. 2020). All sirtuin genes have a conserved catalytic domain and variable carboxy- and amino terminal domains. Most family members possess deacetylase activity, while others have, in addition to weak deacetylase activity, other enzymatic activities like ADP-ribosyltransferase, desuccinylase and demalonylase (Fig. 1). Further, they are located in different subcellular compartments and associated to different biological functions (Fig. 1).

The evolution of the sirtuin genes is an open question. There are multiple phylogenetic hypotheses describing evolutionary relationships among the paralogs in the sirtuin gene family (Frye 2000; North and Verdin 2004; Frye 2006; Greiss and Gartner 2009; Pereira et al. 2011; Slade et al. 2011; Vassilopoulos et al. 2011; Costantini et al. 2013; Scholte et al. 2017; Simó-Mirabet et al. 2017; Yang et al. 2017; Rajabi et al. 2018; Kabiljo et al. 2019; Zhao et al. 2019). Differences in the taxonomic sampling, number of paralogs included, and the inclusion of outgroups, are likely contributors to this variation.

Additionally, studies that are focused on resolving evolutionary relationships are scarce, and in fact, most phylogenetic analyses for sirtuin genes are part of studies where the sirtuin duplicative history is a secondary goal. Additionally, and probably for similar reasons, there are no systematic efforts to characterize the full complement of sirtuin genes among vertebrates. Thus, unraveling the evolutionary history of sirtuin genes represents a challenging and exciting task with a wide range of implications. Because of their role in the aging process, these genes are of great interest. In addition to exploring fundamental questions about the origin and evolution of sirtuin genes, disentangling their evolution is also critical to understanding the diversification of functional and structural phenotypes present in the sirtuin gene family.

This study aims to take advantage of the genomic data available in public databases to advance our understanding of the diversity of vertebrate sirtuin genes and to infer its duplicative history. We also aim to characterize the subcellular localization, enzymatic activity, and mitochondrial activity of the newly discovered *SIRT8* gene lineage in the elephant shark (*Callorhinchus milii*) as a representative species. Our phylogenetic tree is in general well resolved, recovering vertebrate sirtuin genes into three clades: 1) *SIRT4*, *SIRT5*, 2) *SIRT6* and *SIRT7*, and 3) *SIRT1*, *SIRT2*, *SIRT3*, and *SIRT8*. The new sirtuin family member (*SIRT8*) is retained in all vertebrates other than amniotes (the group that includes mammals, birds, and reptiles). Based on how sirtuin genes are related to each other and the information is already known for the other sirtuin family members, we can predict that SIRT8 belongs to the class I, has a deacetylase activity, and is mainly located on mitochondria. Our experimental analyses confirmed our evolutionary guided inferences.

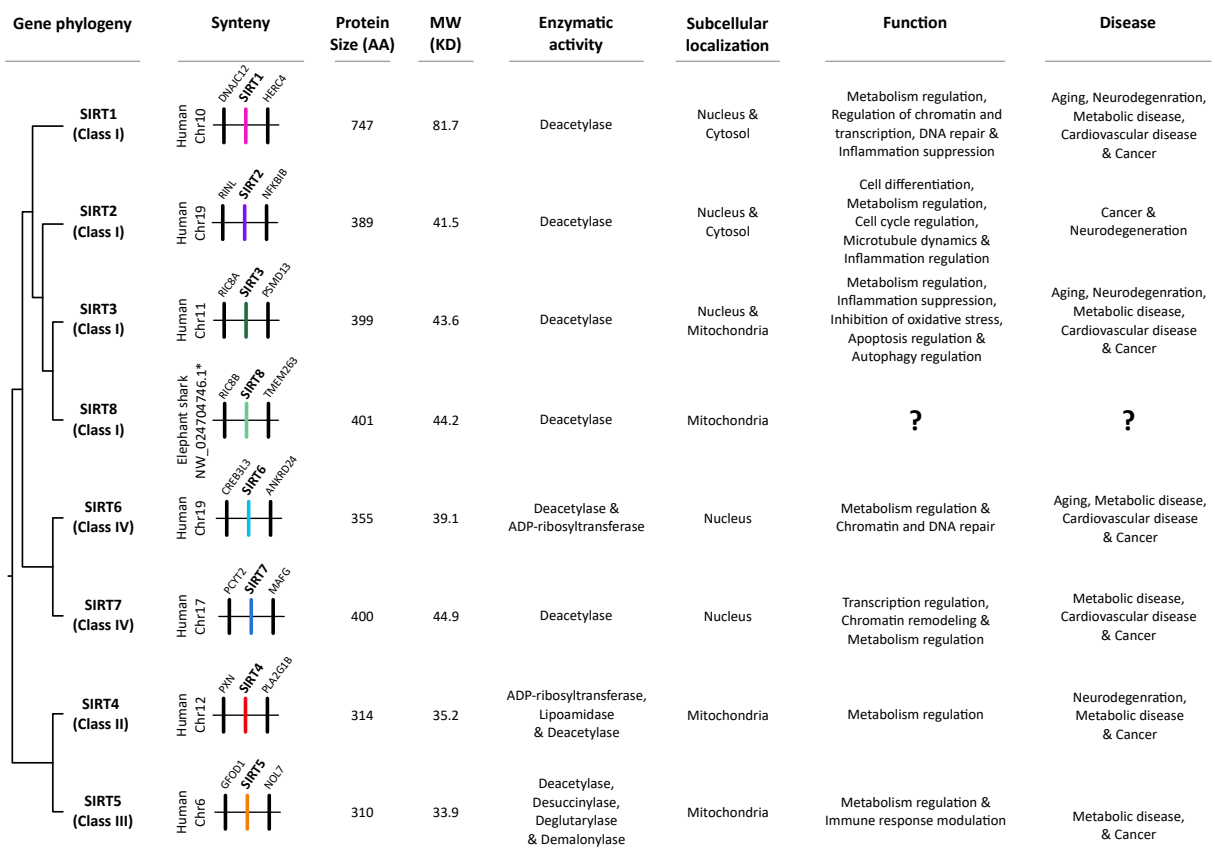

Figure 1. Gene phylogeny, synteny, protein size, molecular weight, enzymatic activity, subcellular localization, functions and diseases associated with sirtuin genes. Information regarding the sister group relationships among sirtuin genes was obtained from this study, synteny from ENSEMBL v.106 (Howe et al. 2021), protein size from Fujita and Yamashita (2018)(Fujita and Yamashita 2018), molecular weight from Vassilopoulos et al. (2011)(Vassilopoulos et al. 2011) while enzymatic activity, subcellular localization, functions and diseases from Zhang et al. (2020)(Zhang et al. 2020). In the case of the *SIRT8* of the elephant shark, synteny information was obtained from the National Center for Biotechnology Information (NCBI) (Sharma et al. 2019), protein size, molecular weight, enzymatic activity and subcellular localization from this study.

Results and Discussion

Vertebrate sirtuin paralogs are recovered into two main clades

We recovered the monophyly of all sirtuin family members with strong support (Fig. 2). The diversity of sirtuin genes was arranged into three main clades (Fig. 2). The first clade contains the SIRT4 and SIRT5 paralogs, the second clade contains the SIRT6 and SIRT7 paralogs, and the third clade includes the SIRT1, SIRT2, SIRT3 and SIRT8 gene lineages (Fig. 2). A diversity of phylogenetic arrangements for sirtuin genes have been

138 proposed in the past (Frye 2000; Frye 2006; Greiss and Gartner 2009; Slade et al. 2011;
139 Vassilopoulos et al. 2011; Costantini et al. 2013; Scholte et al. 2017; Simó-Mirabet et al.
140 2017; Yang et al. 2017; Rajabi et al. 2018; Kabiljo et al. 2019; Zhao et al. 2019), and our
141 results largely support the relationships proposed by Frye (2006).

142 In the first clade we recovered the sister group relationships between SIRT4 and
143 SIRT5 with strong support (Fig. 2). Evolutionary relationships between these two family
144 members are still a matter of debate, as a variety of phylogenetic positions have been
145 suggested for these paralogs (Slade et al. 2011; Vassilopoulos et al. 2011; Costantini et
146 al. 2013; Yang et al. 2017; Rajabi et al. 2018), and only in a fraction of the studies their
147 sister group relationship is supported (Frye 2000; North and Verdin 2004; Frye 2006;
148 Greiss and Gartner 2009; Hirschey 2011; Scholte et al. 2017; Simó-Mirabet et al. 2017;
149 Kabiljo et al. 2019; Zhao et al. 2019). In the second clade, we recovered SIRT6 sister to
150 the clade containing SIRT7 sequences with strong support (Fig. 2). The sister group
151 relationship between SIRT6 and SIRT7 has been recovered in all examined studies (Frye
152 2000; North and Verdin 2004; Greiss and Gartner 2009; Hirschey 2011; Slade et al.
153 2011; Vassilopoulos et al. 2011; Costantini et al. 2013; Scholte et al. 2017; Simó-Mirabet
154 et al. 2017; Yang et al. 2017; Rajabi et al. 2018; Kabiljo et al. 2019; Zhao et al. 2019),
155 suggesting there is robust support for the sister relationship between these sirtuin family
156 members. In the third clade, there is a broad consensus in the literature that SIRT2
157 shares a common ancestor more recently in time with SIRT3 than with any other sirtuin
158 paralog, and that the clade containing SIRT1 sequences is sister to the SIRT2/SIRT3
159 clade (Frye 2000; North and Verdin 2004; Frye 2006; Greiss and Gartner 2009; Hirschey
160 2011; Slade et al. 2011; Vassilopoulos et al. 2011; Costantini et al. 2013; Scholte et al.
161 2017; Simó-Mirabet et al. 2017; Yang et al. 2017; Rajabi et al. 2018; Zhao et al. 2019).
162 We recovered the same evolutionary relationships with strong support (Fig. 2). The
163 sister-group relationship between the SIRT6/SIRT7 and SIRT2/SIRT3/SIRT8/SIRT1
164 received moderate support (Fig. 2). The sister-group relationships among the three main
165 sirtuin clades is something that has been difficult to resolve (Simó-Mirabet et al. 2017;
166 Zhao et al. 2019), as it appears divergences were close in time, as evidence by the short
167 length of the corresponding branch (Fig. 2).

168 In summary, we present a phylogenetic analysis based on a taxonomic sampling that
169 included representative species from all main groups of vertebrates for all sirtuin family
170 members. Our phylogenetic tree is in general well resolved (Fig. 2), representing an
171 advance in our understanding of the duplicative history of the sirtuin gene family. In
172 comparison to the phylogenetic trees currently available in the literature only one study
173 shows the same topology as our study (Frye 2006).

174

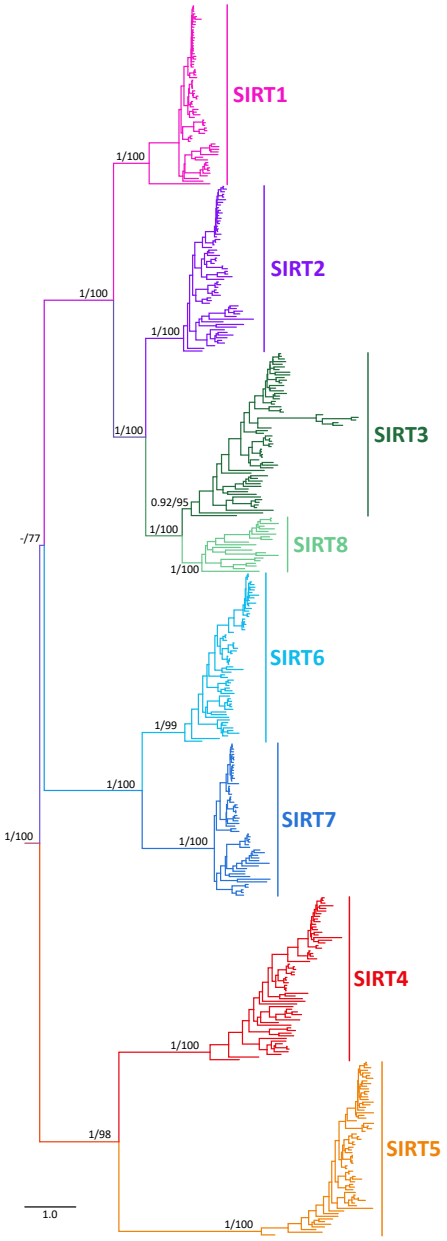

175

Figure 2. Maximum likelihood tree showing sister group relationships among sirtuin genes of vertebrates. Numbers on the nodes correspond to support from the aBayes and ultrafast bootstrap values. Nicotinamide Nucleotide Transhydrogenase (NNT) sequences from the human (*Homo sapiens*) mouse (*Mus musculus*), spotted gar (*Lepisosteus oculatus*) and zebrafish (*Danio rerio*) were used as outgroups (not shown). The scale denotes substitutions per site and colors represent vertebrate sirtuin lineages.

Identification of a new sirtuin gene family member, *SIRT8*

In our analyses, we identified a new sirtuin family member (Fig. 2 and 3), *SIRT8*, which is present in a fraction of the vertebrate tree of life (Fig. 4) that was recovered sister to the *SIRT3* clade with strong support (Fig. 2 and 3). Synteny conservation provides further support to the monophyly of the *SIRT8* gene lineage in gnathostomes (Fig. 5a), as genes found at the 5` side (*POLR3B*, *RFX4* and *RIC8B*) and 3` side (*TMEM263*, *MTERF2*, and *CRY1*) of the *SIRT8* gene are well conserved (Fig. 5a). Synteny is also conserved in species in which the *SIRT8* gene was lost (Fig. 5a). Among vertebrates, we found orthologs of the *SIRT8* gene in representative species of cartilaginous fish, bony fish, coelacanth, and amphibians (Fig. 4). A comparison of the genomic region of the tropical clawed frog (*Xenopus tropicalis*), which possesses the *SIRT8* gene, with the corresponding region in the human (*Homo sapiens*), opossum (*Monodelphis domestica*), chicken (*Gallus gallus*), gharial (*Gavialis gangeticus*), red-eared slider (*Trachemys scripta*) and green anole (*Anolis carolinensis*) strongly suggests that the *SIRT8* gene is not present in the vertebrate lineages that these species represent (Fig. 5b). The absence of the *SIRT8* gene in mammals, birds and reptiles indicates that it was probably lost in the common ancestor of the group, between 352 and 312 millions of years ago (Kumar et al. 2017). In the case of cyclostomes, we found in the sea lamprey (*Petromyzon marinus*) a chromosomal region (Chr3) that possess *TMEM263* and *POLR3B* separated by 44 base pairs, suggesting that all the genes that should be in between (*RFX4*, *RIC8B*, *SIRT8*) were lost in cyclostomes. Alternatively, it is possible that *SIRT8*, and all the other genes are present in cyclostome genomes, but not in the current genome assembly. In the past, Pereira et al. (2011), with a limited taxonomic sampling, identified a clade sister to a group containing *SIRT3* sequences. This gene lineage included sequences from three species with an evolutionary history of whole-genome duplications, two teleost fish (zebrafish, *Danio rerio*, and green spotted puffer, *Tetraodon nigroviridis*), and one

209 amphibian (African clawed frog, *Xenopus laevis*), complicating the definition of their
210 duplicative history. Thus, our results, including a balanced taxonomic sampling of all main
211 vertebrate groups and appropriate phylogenetic searches, define the existence of the
212 *SIRT8* gene lineage and its phyletic distribution.
213

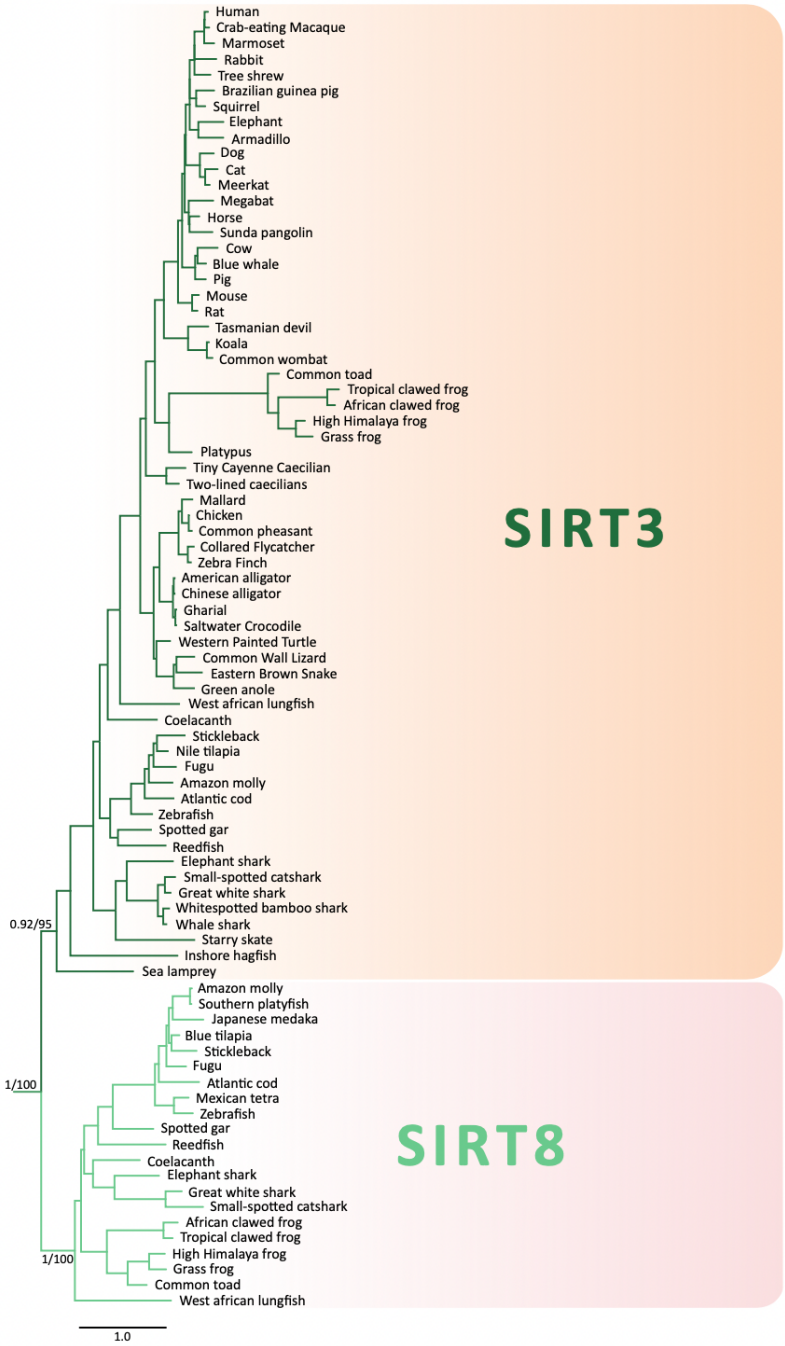

214
215

Figure 3. Maximum likelihood tree showing sister group relationships among *SIRT3* and *SIRT8* genes in vertebrates. Numbers on the nodes correspond to support from the aBayes and ultrafast bootstrap values. The scale denotes substitutions per site and colors represent gene lineages. This tree does not represent a novel phylogenetic analysis, it is the *SIRT3*/*SIRT8* clade that was recovered from figure 2.

The lack of the *SIRT8* gene can be interpreted in different ways. We can think that the loss of *SIRT8* could have no physiological impact if the functional role of the lost gene is assumed by other family members, consistent with the idea that gene families possess functional redundancy (Ohno 1985; Félix and Barkoulas 2015; Albalat and Cañestro 2016). Alternatively, we can also think of gene loss as a source of adaptive evolution (Olson 1999; Albalat and Cañestro 2016; Helsen et al. 2020). The description of new gene lineages is not uncommon in the literature (Wichmann et al. 2016; Himmel et al. 2020; Opazo et al. 2021). It could be mainly attributed to the presence in non-model species and/or the absence of proper evolutionary analyses. The existence of species with different gene repertoires is an opportunity to better understand the evolutionary fate of duplicated genes (Lynch and Conery 2000) and the biological functions associated to a group of genes.

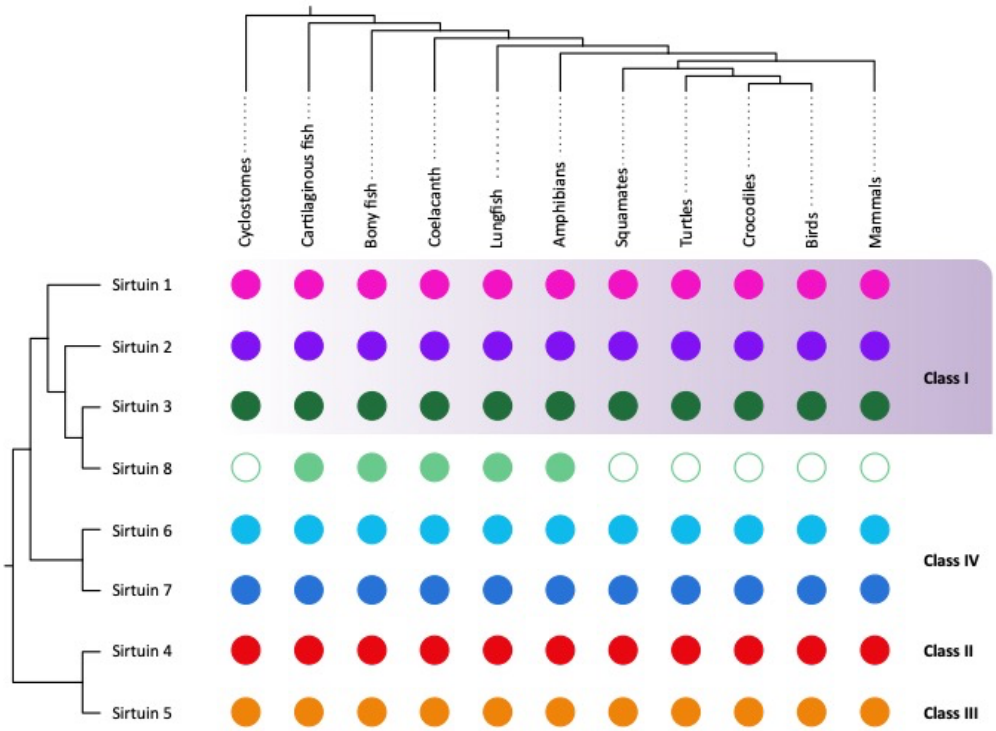

Figure 4. Phyletic distribution of sirtuin genes in vertebrates. The sister group relationships among sirtuin genes was obtained from this study, whereas, organismal phylogeny was obtained from the most updated phylogenetic hypotheses available in the literature (Iwabe et al. 2005; Delsuc et al. 2006; Delsuc et al. 2008; Hara et al. 2018). The colors of the circles are those used in figure 2 to define sirtuin gene lineages, whereas the classes to which the different sirtuins belong are shown with shading.

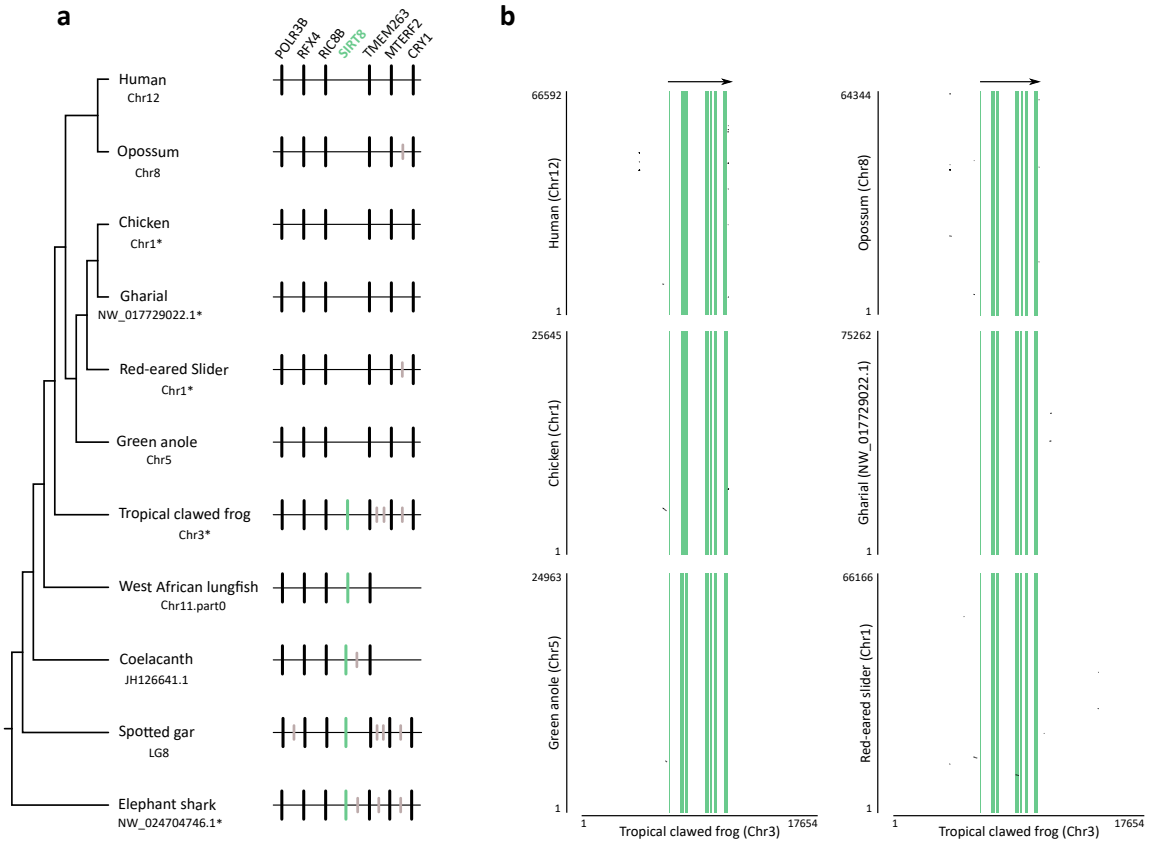

Figure 5. a Patterns of conserved synteny in the chromosomal region that harbor SIRT3-like genes in gnathostomes. Asterisks denote that the orientation of the genomic piece is from 3´ to 5´, gray lines represent intervening genes that do not contribute to conserved synteny. **b** Pairwise dot-plot comparison of the genomic region of the tropical clawed frog (*Xenopus tropicalis*) with the corresponding region in the human (*Homo sapiens*), opossum (*Monodelphis domestica*), chicken (*Gallus gallus*), gharial (*Gavialis gangeticus*), red-eared slider (*Trachemys scripta*) and green anole (*Anolis carolinensis*). Light green vertical lines denote exons and regions in between are introns. Dot plots were based on the complete coding region in addition to 6.7 kb of upstream and downstream flanking sequence. The genome assembly version of the species depicted in this figure is the following: Human: GRCh38.p13; Opossum: ASM229v1; Chicken: GRCg6a; Gharial: GavGan_comp1; red-eared slider: CAS_Tse_1.0; Green anole: AnoCar2.0v2; Tropical clawed frog: UCB_Xtro_10.0; Coelacanth: LatCha1; Spotted gar: LepOcu1 and Elephant shark: Callorhinchus_milii-6.1.3.

An amino acid alignment of the SIRT8 and SIRT3 sequences shows that the catalytic domain of SIRT8 is well conserved, where six amino acid positions were identified as diagnostic characters (Fig. 6). The amino acid divergence of the SIRT8

catalytic domain varies from 32.2% (spotted gar vs coelacanth) to 33.6% (spotted gar vs elephant shark). The same comparisons for the SIRT3 catalytic domain show slightly lower amino acid divergence values, between 24.8% (spotted gar vs coelacanth) and 31.0% (coelacanth vs elephant shark). As expected, the interparalog distance (SIRT3 vs SIRT8) of the catalytic domains shows higher divergence values, ranging from 40.7% (spotted gar SIRT3 vs spotted gar SIRT8) and 43.6% (elephant shark SIRT3 vs elephant shark SIRT8). Although nothing is known about the protein encoded by the SIRT8 gene, based on how sirtuin genes are evolutionarily related and the information already known for the other family members (Fig. 1), we can speculate that SIRT8 belongs to the class I, is mainly located on the mitochondria/nucleus, and has deacetylase activity. From a functional perspective it should perform functions similar to what has been described for SIRT3 (Fig. 1) (Brown et al. 2013; McDonnell et al. 2015; Zhang et al. 2020). It is important to highlight that the inferences regarding a newly discovered gene are better performed if they are phylogenetically guided.

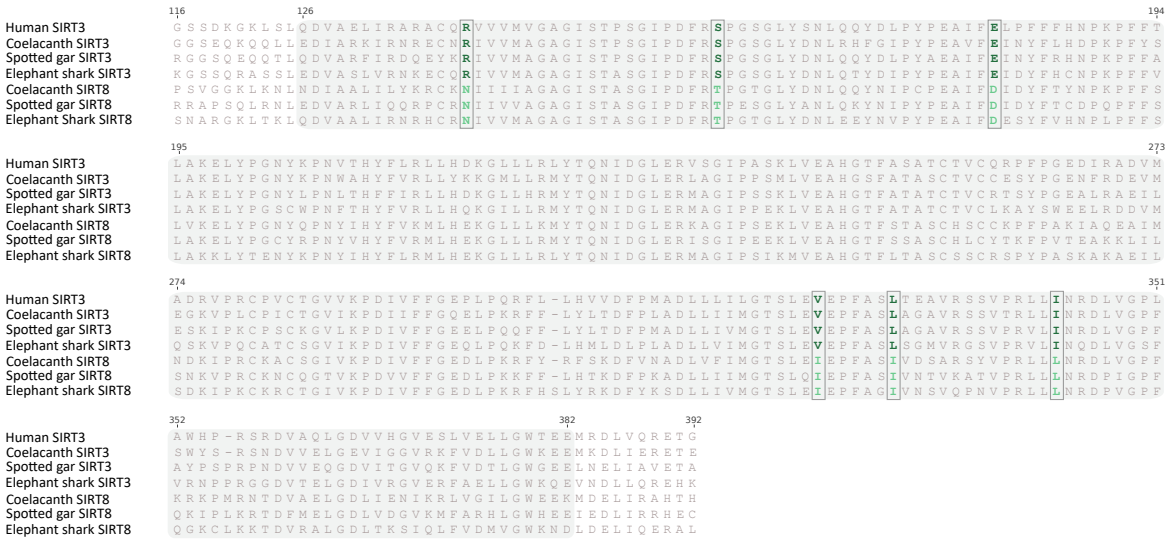

Figure 6. Alignment of the catalytic domain of SIRT3 in humans (*Homo sapiens*), and SIRT3 and SIRT8 of spotted gar (*Lepisosteus oculatus*), coelacanth (*Latimeria chalumnae*) and elephant shark (*Callorhinchus milii*). The shaded region denotes the catalytic domain. Diagnostic characters -i.e. amino acids positions that distinguish between SIRT3 and SIRT8 gene lineages - are indicated with a rectangle and green colors.

287 ## Expression pattern of sirtuin gene family members

288 Our next step in characterizing the *SIRT8* gene was to investigate whether it is
289 transcribed and if it was, to characterize the transcription pattern. To do this, we mapped
290 RNASeq reads to reference gene sequences of representative species of vertebrates and
291 examined transcript abundance. In agreement with the transcription pattern reported for
292 sirtuin genes (Stelzer et al. 2016; Kabiljo et al. 2019), our results show that although they
293 exhibited wide variance in tissue expression, sirtuin genes are expressed in almost all
294 tissues, including the novel *SIRT8* gene lineage (Fig. 7). In the case of the tropical clawed
295 frog, the *SIRT8* gene is transcribed at a similar level in all tissues, other than the ovary
296 where high transcription levels were estimated (Fig. 7). Coincident with the pattern
297 observed in the tropical clawed frog, the elephant shark *SIRT8* gene is mostly transcribed
298 in the ovary (Fig. 7). These results should be taken with caution given the lack of biological
299 replicates, at least within species. In the case of the zebrafish, although our transcription
300 level estimations did not follow the trend previously mentioned, an extensive study
301 examining the expression of all sirtuin genes in zebrafish showed that the *SIRT8* gene in
302 this species is mainly expressed in the ovary (Pereira et al. 2011). Thus, in addition to
303 showing that the *SIRT8* gene is transcribed, our analyses allow us to suggest that this
304 gene could be involved in biological processes associated with reproduction. This
305 observation agrees with the literature as for SIRT3 there are many studies in which its
306 functions related to reproduction have been reported (Zhao et al. 2016; Tatone et al. 2018;
307 Vazquez et al. 2020; Di Emidio et al. 2021).

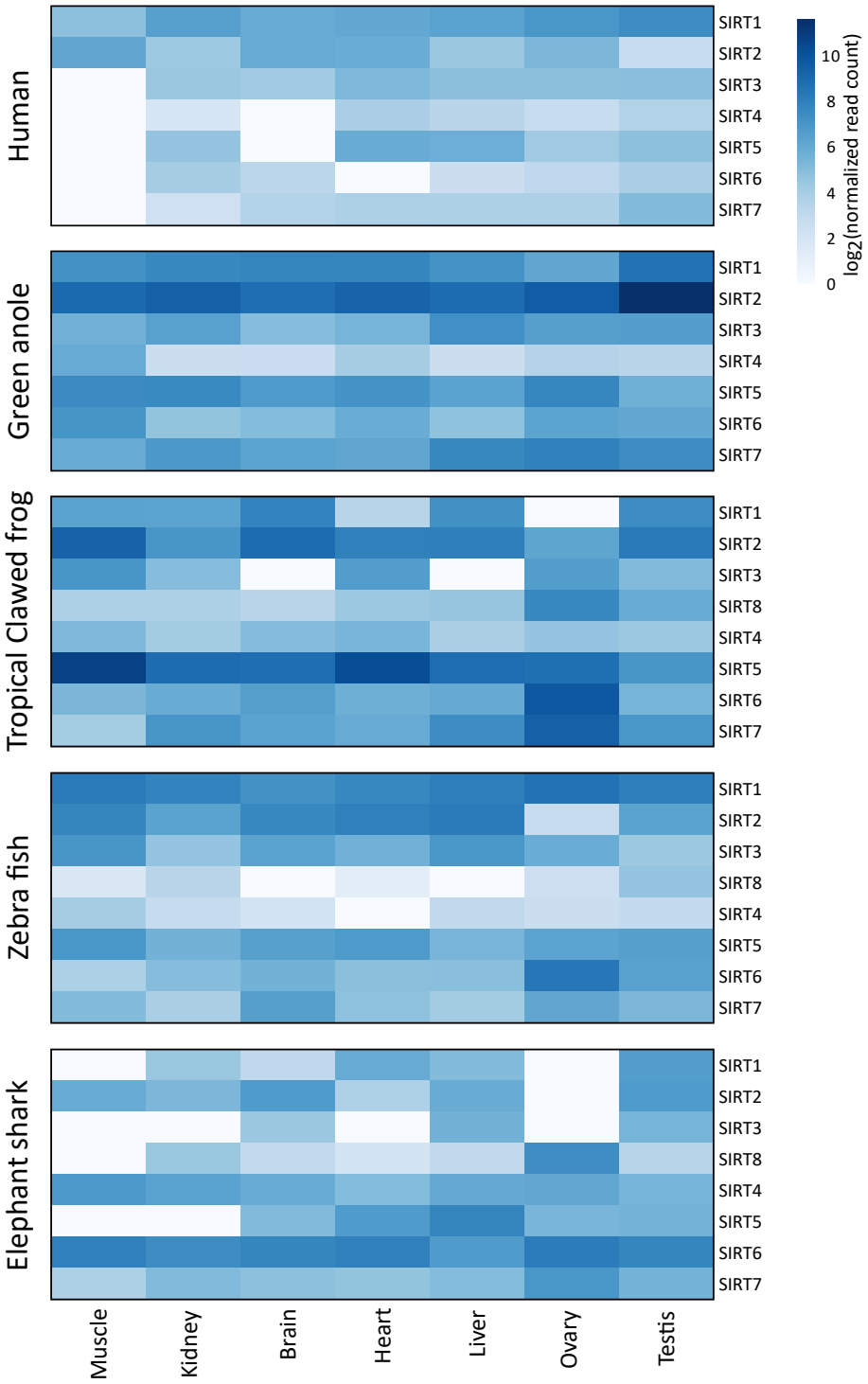

Figure 7. Heatmap representation of within-species relative transcriptional levels of sirtuin paralogs between 7 chosen tissues. Transcription values were calculated independently for each species and normalized over all tissues.

Elephant shark SIRT8 protein localizes to mitochondria

To further explore the structural relationship between SIRT3 and SIRT8 proteins, we performed an unbiased protein structure modeling of SIRT8 proteins from elephant shark (*Callorhinchus milii*), spotted gar (*Lepisosteus oculatus*), salmon (*Salmo salar*) and coelacanth (*Latimeria chalumnae*). Models of SIRT8 proteins were generated by the SWISS-MODEL workspace that used as template crystal structure models of human SIRT3: 4bvh.1.A for elephant shark, 5z94.1.A for spotted gar, 5d7n.3.A for salmon and 5bwo.1.B for coelacanth (data not shown). All models generated comprise only the central portion of the SIRT8 proteins where the catalytic and its regulatory regions are expected to be: amino acids G95 to Q365 for elephant shark, L115 to V388 for spotted gar, P114 to G387 for salmon, and K113 to P386 for coelacanth. The overall root mean square deviation for 272 superimposable Cα coordinates for the models of human SIRT3 (pdb: 4bvh.1.A; amino acids G121 to G392) and elephant shark SIRT8 (amino acids G95 to Q365) is 0.101 Å (Fig. 8a), suggesting extensive structural match. Some SIRT proteins, such as SIRT1, SIRT2 and SIRT3, possess evolutionarily conserved, distinct cellular localizations and functions, as evidenced by their analysis in several model species that include Drosophila melanogaster, Mus musculus and Homo sapiens (McBurney et al. 2003; Blander and Guarente 2004; North and Verdin 2004; Michishita et al. 2005; Haigis et al. 2006) (Fig. 1). Some sirtuins localize in more than one compartment, like SIRT1 and SIRT2 that localize to the nucleus and cytosol, and SIRT3 that localizes mainly to the mitochondrial matrix, but with a small fraction localizing to the nucleus (Scher et al. 2007). In contrast, SIRT4 and SIRT5 localize only to mitochondria, and SIRT6 and SIRT7 localize only to the nucleus. The sequence and structural comparison between SIRT8 and SIRT3 proteins, as well as subcellular localization prediction by LocTree3 (Goldberg et al. 2014), suggest that the localization of SIRT8 proteins is also in the mitochondria. To determine the subcellular localization of SIRT8 proteins, we chose to analyze SIRT8 from elephant shark. To this end, we expressed in human cultured cells full-length elephant shark SIRT8 tagged with three copies of the c-Myc epitope at the C-terminus (SIRT8-3myc). To obtain biochemical evidence of the expression of this protein, we

341 performed immunoblot analysis with monoclonal antibody 9E10 against the c-Myc
342 epitope, which showed the detection of an expected 48.3 kDa protein in all cell lines
343 analyzed (Fig. 8b). Fluorescence microscopy analysis of human H4 neuroglioma cells
344 expressing SIRT8-3myc showed decoration by the anti-c-Myc antibody of structures
345 highly reminiscent of mitochondria, in addition to a faint fluorescent signal in the rest of
346 the cytoplasm (Fig. 8c, d). Mitochondria localization of SIRT8-3myc was confirmed by co-
347 localization with the fluorescent signal of MitoTracker Orange (Pearson's correlation
348 coefficient [r] = 0.94 ± 0.02; *n* = 20; Fig. 8c and Supplementary Fig. 1a). Importantly,
349 SIRT8-3myc showed no localization in any other major compartment, as shown by lack
350 of localization in the nucleus (detected with the nuclear stain DAPI; r = 0.21 ± 0.03; *n* =
351 20; Fig. 8c, d and Supplementary Fig. 1b), the Golgi apparatus (detected with antibody
352 against Trans-Golgi network integral membrane protein 2 (TGN46) (Ponnambalam et al.
353 1996) (r = 0.34 ± 0.09; *n* = 20; Fig. 8c, d and Supplementary Fig. 1c), or the endoplasmic
354 reticulum (detected with antibody against Cytoskeleton-associated protein 4 (P63)
355 (Schweizer et al. 1993) (r = 0.47 ± 0.15; *n* = 20; Fig. 8d and Supplementary Fig. 1d). The
356 same pattern of expression of SIRT8-3myc was obtained using other human cell lines,
357 such as HeLa or MDA-MB-231 cells (data not shown). Altogether, these results indicate
358 that SIRT8 proteins are targeted to the mitochondria.

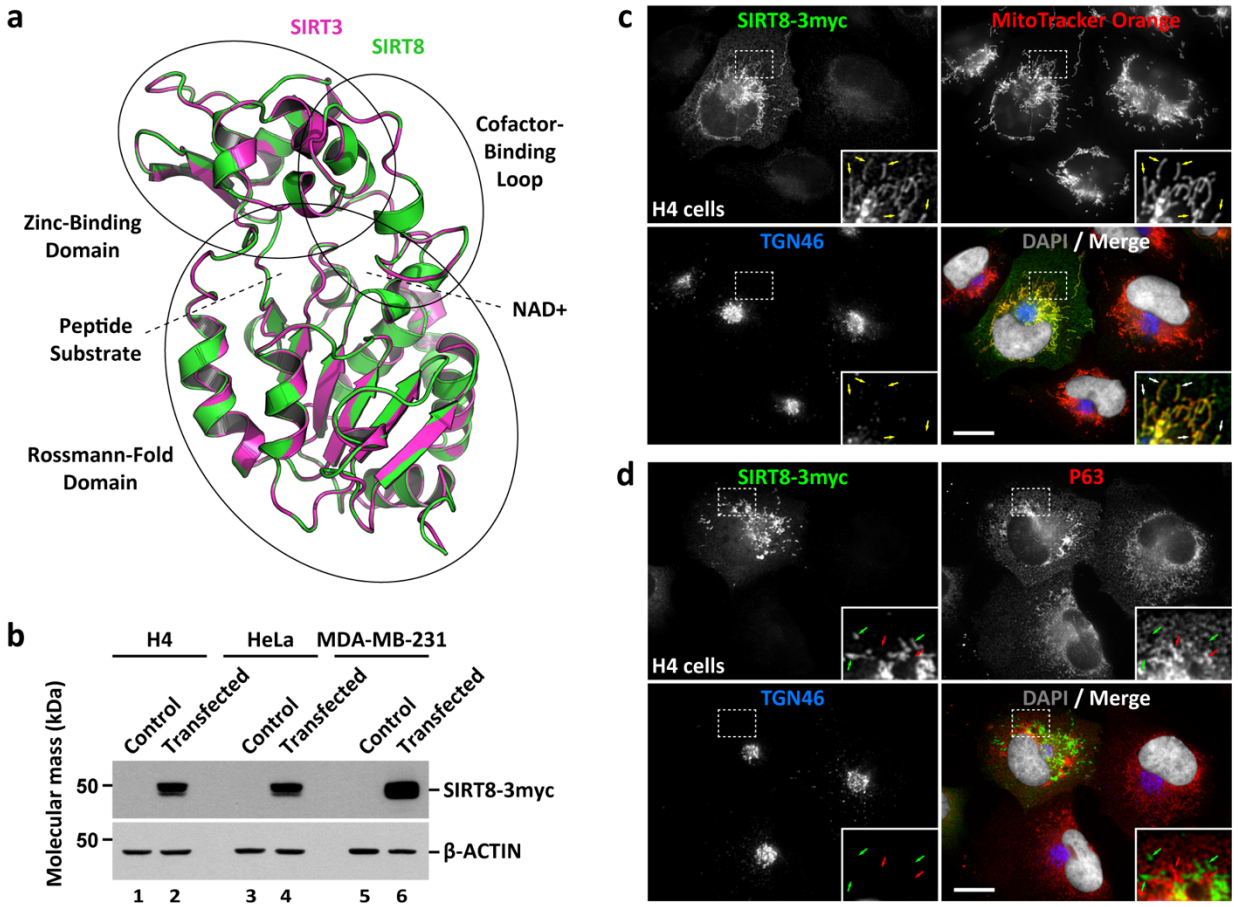

Figure 8. Structural model of elephant shark SIRT8 and expression of SIRT8-like-3myc in mammalian cells. **a** Superposition of the ribbon representations of elephant shark SIRT8 (green model; amino acids G95 to Q365) and human SIRT3 (magenta model; pdb: 4bvh.1.A; amino acids G121 to G392). Depicted in ellipses are the indicated functional/structural domains of SIRT3 and in dotted lines the binding sites for peptide substrates and NAD^+. **b** The indicated cells were left untreated (Control, lanes 1, 3 and 5) or transfected to express SIRT8-3myc (lanes 2, 4 and 6), followed by immunoblot analysis with antibody against the c-Myc epitope or antibody against β-ACTIN used as loading control. The position of molecular mass markers is indicated on the left. SIRT8-3myc exhibits an electrophoretic mobility corresponding to a protein of 48.3 kDa, which is expected considering the extra amino acids of the three copies of the c-Myc epitope at the C-terminus. **c** and **d** H4 cells grown in glass coverslips were transfected to express SIRT8-3myc (green channel) and incubated with the mitochondrial probe MitoTracker Orange (red channel in c) or mock incubated (d). Cells were fixed, permeabilized, and double- (c) or triple-labeled (d) with mouse monoclonal antibody against the c-Myc epitope (c and d), rabbit polyclonal antibody against the endoplasmic reticulum protein Cytoskeleton-associated protein 4 (P63; d) and sheep polyclonal antibody against the Golgi apparatus protein Trans-Golgi network integral membrane protein 2 (TGN46; c and d). Secondary antibodies were Alexa-Fluor-488-conjugated donkey anti-mouse IgG (green channel), Alexa-Fluor-594-conjugated donkey anti-rabbit IgG (red channel), and Alexa-Fluor-647-conjugated donkey anti-sheep IgG (blue channel), and nuclei were

stained with the DNA probe DAPI (white channel). Stained cells were examined by fluorescence microscopy. Insets: X3 magnification with yellow arrows indicating colocalization (c) and green and red arrows indicating lack of colocalization (d). Bar, 10 µm.

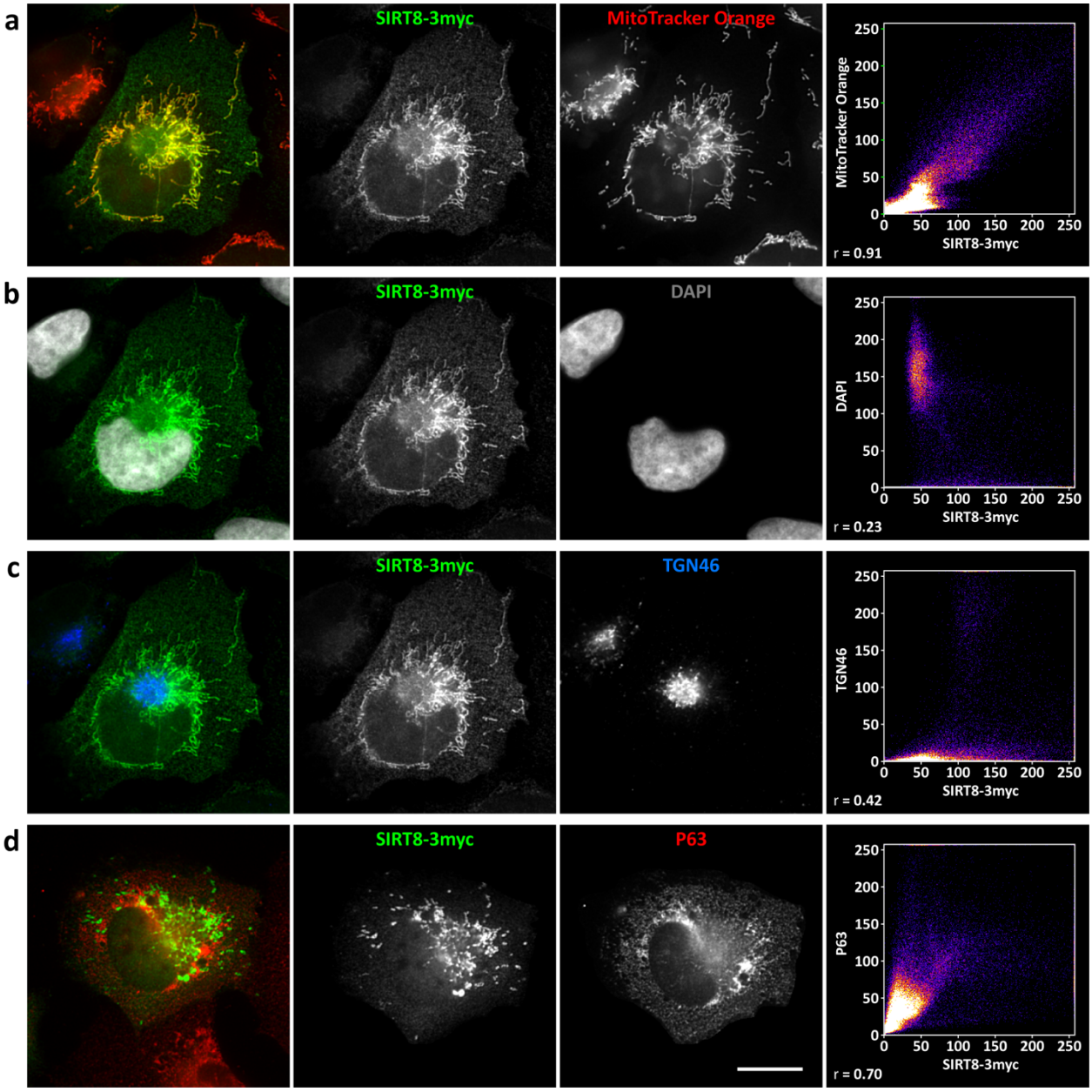

Supplementary Figure 1. Colocalization analysis of the immunofluorescence detection of SIRT8-3myc. H4 cells were processed as indicated in Figure legend 8c and 8d. The figure shows a representative colocalization analysis between the fluorescent signals of SIRT8-3myc and the mitochondrial probe MitoTracker Orange (a), SIRT8-3myc and the nuclear probe DAPI (b), SIRT8-3myc and antibody against the Golgi apparatus protein Trans-Golgi network integral membrane protein 2 (TGN46; c), and SIRT8-3myc and

393 antibody against the endoplasmic reticulum protein Cytoskeleton-associated protein 4
394 (P63; d). The first column shows the overlapping of corresponding second and third
395 images in each row. The fourth column shows the corresponding two-dimensional
396 cytofluorograms of the colocalization analysis using the plugin JACoP implemented in the
397 software ImageJ (version 1.47h). The corresponding Pearson's correlation coefficient is
398 indicated in the bottom left corner of the cytofluorograms. Diagonal in a cytofluorogram
399 indicates high degree of colocalization. Bar, 10 μm.
400

401 Elephant shark SIRT8 protein has deacetylase activity

402 Reversible lysine acetylation is one of the most common post-translational modifications
403 on proteins that regulate a variety of physiological processes including gene expression,
404 enzymatic activity, protein-protein interactions, and subcellular localization (Glozak et al.
405 2005). Sirtuin proteins share a catalytic core domain (North and Verdin 2004) that have
406 NAD^+-dependent deacetylase activity (Shahgaldi and Kahmini 2021). After translocation
407 into the mitochondrial matrix, human SIRT3 is inactive, but after proteolytic processing of
408 its N-terminus signal peptide it becomes active as deacetylase (Onyango et al. 2002;
409 Schwer et al. 2002). Similar to human SIRT3, secondary structure prediction of
410 representative SIRT8 proteins indicates that the first ~100 N-terminal amino acids are in
411 a disordered domain (data not shown). Therefore, to determine if SIRT8 proteins also
412 exhibit deacetylase activity, we produced in bacteria N-terminal truncated elephant shark
413 SIRT8 protein (amino acids 95-372; **Δ**NT-SIRT8). To analyze the enzymatic activity of
414 purified **Δ**NT-SIRT8, we used a commercial fluorometric deacetylation activity assay that
415 contains an acetylated substrate peptide for recombinant human SIRT3 (Abcam). An
416 initial analysis of activity at 37ºC showed that **Δ**NT-SIRT8 possesses a deacetylase
417 activity that is similar to that of human SIRT3, being also NAD^+-dependent (Fig. 9a, e, f).
418 Because the enzymatic activity of elephant shark SIRT8 could be influenced by the
419 environmental conditions, we next evaluated the optimal temperature of **Δ**NT-SIRT8
420 compared to that of human SIRT3. As expected, the optimal temperature of the human
421 SIRT3 was ~37ºC (Fig. 9b). In contrast, **Δ**NT-SIRT8 exhibited an optimal temperature at
422 ~24ºC (Fig. 9b). The optimal temperature value for the SIRT8 deacetylase activity of the
423 elephant shark could represent an evolutionary adjustment to the temperature regime of
424 the habitat in which this species lives, as it has been demonstrated for other enzymes in
425 other species (McCormick 1993; Somero 2004; Bilyk et al. 2021; Saravia et al. 2021).

426 Thus, all subsequent enzymatic activity analyses for **Δ**NT-SIRT8 were performed at 24ºC.
427 The apparent specific activity of **Δ**NT-SIRT8 was 260.7 ± 9.9 fluorescence units (FU) min^{-}
428 ^{1} mg^{-1}, which was significantly lower than that of SIRT3 that was 1143.3 ± 46.3 FU min^{-1}
429 mg^{-1}. Apparent K_m of **Δ**NT-SIRT8 and SIRT3 were 5.7 and 5.5, respectively, which
430 resulted not significantly different (Fig. 9c, d). In contrast, apparent V_{max} of **Δ**NT-SIRT3-
431 like was 0.322 FU sec^{-1}, which was significantly different to that of SIRT3 that was 3.908
432 FU sec^{-1} (Fig. 9c, d). We next compared the effect of the sirtuin inhibitors nicotinamide
433 (NAM) (Sauve and Schramm 2003) and quercetin (QUE) (You et al. 2019) on the activities
434 of SIRT3 and **Δ**NT-SIRT8. As expected, SIRT3 activity was significantly inhibited by NAM
435 and QUE (Fig. 9e). We also found a significant inhibitory effect of both NAM and QUE on
436 the activity of **Δ**NT-SIRT8 (Fig. 9f). We also compared the effect of the polyphenolic
437 antioxidant resveratrol (REV), which is an activator of sirtuins (Wood et al. 2004). As
438 expected, we found a significant concentration-dependent activation of SIRT3
439 deacetylase activity up to a 1.6 ± 0.1-fold increase in the presence of 100 μM REV (Fig.
440 9e). Strikingly, we found a much more potent concentration dependent activation effect
441 of REV on **Δ**NT-SIRT8, showing up to a 11.1 ± 0.6 fold increase in the presence of 100
442 μM REV (Fig. 9f). However, because the specific activity of **Δ**NT-SIRT8 was ~23% that of
443 SIRT3 in the assay conditions, the activation of **Δ**NT-SIRT8 by REV in fact represents a
444 value only ~1.6 fold higher compared to the activation of SIRT3 by REV. Because different
445 sirtuins have activity on different proteins, as well as remove with different specificity a
446 variety of acyl groups other than the acetyl (Fig. 1) (Anderson et al. 2014), the modulation
447 of **Δ**NT-SIRT8 activity by REV suggests that it has distinct functional substrates. Together,
448 these results demonstrate that elephant shark **Δ**NT-SIRT8 has deacetylase activity and
449 indicate that the activity of SIRT8 proteins is modulated in a similar manner to that of
450 mammalian sirtuins.

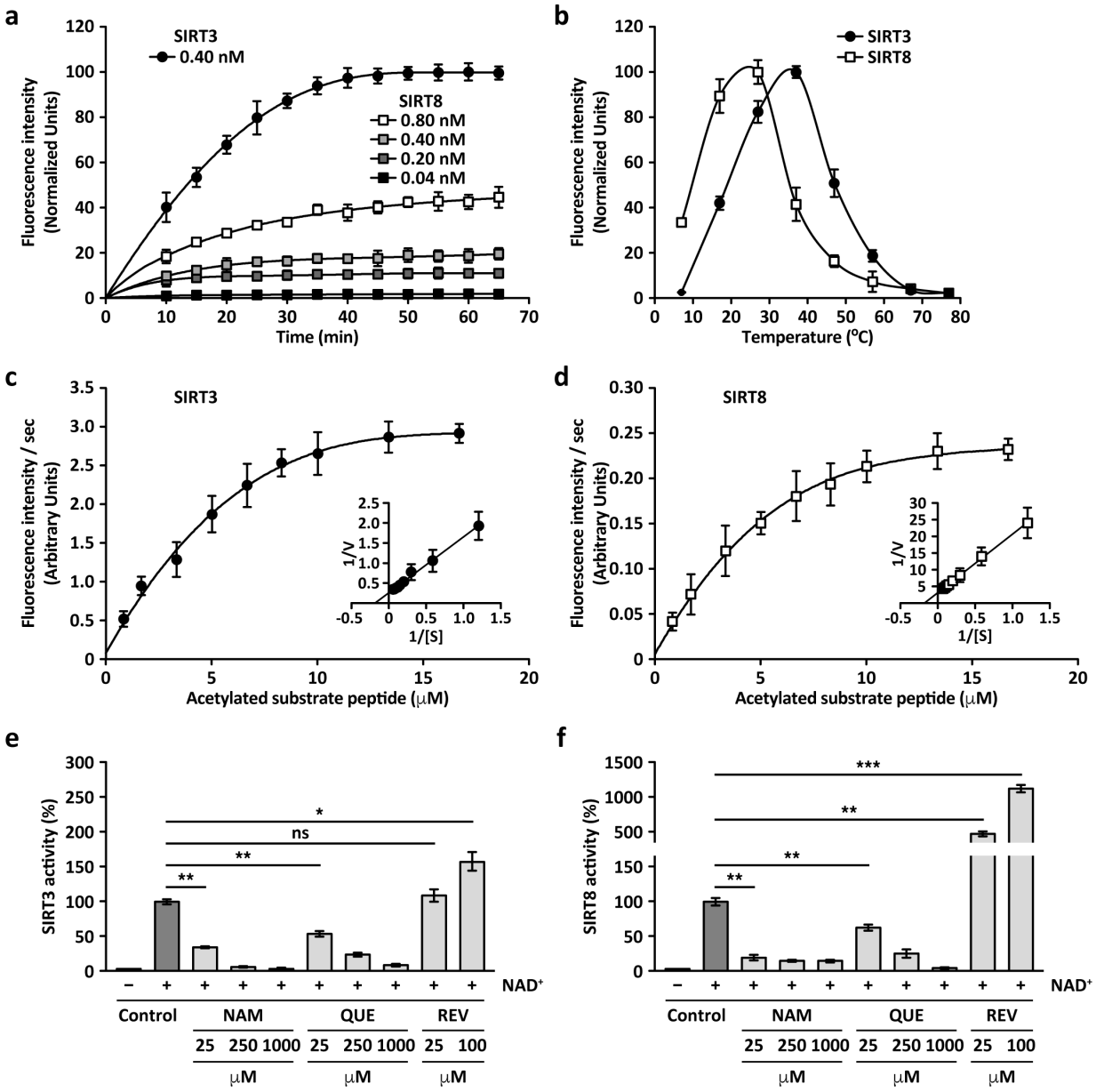

Figure 9. Comparison of deacetylase activity between human SIRT3 and elephant shark **Δ**NT-SIRT8. a-f) Results obtained with a fluorometric deacetylation assay of an acetylated substrate peptide. a) Time course of deacetylase activity at the indicated concentration of SIRT3 and concentrations of **Δ**NT-SIRT8. b) Temperature dependence of deacetylase activity. c-d) Michaelis-Menten plot and Lineweaver-Burk plot of SIRT3 (c) and **Δ**NT-SIRT8 (d) deacetylase activity. e-f) NAD^+ dependence and concentration dependent effects of the SIRT3 inhibitors nicotinamide (NAM) and quercetin (QUE) and of the SIRT3 activator resveratrol (REV) on the deacetylase activity of SIRT3 (e) and **Δ**NT-SIRT8 (f). In a-d, graphs depict the mean ± standard deviation (n = 3). In e-f, bars represent the mean ± standard deviation. Statistical analysis was performed using two-tailed unpaired Student's t-test (n = 3; * $p < 0.05$; ** $p < 0.01$; *** $p < 0.001$; ns, not statistically significant).

464 ## Elephant shark SIRT8 protein increases ATP cellular content

465 Considering that SIRT3 plays an important role in maintaining basal ATP levels by
466 deacetylation of mitochondrial proteins involved in electron transport chain (ETC), the
467 tricarboxylic acid cycle, and fatty-acid oxidation (Hirschey et al. 2010), we investigated
468 the impact of transient SIRT8-3myc expression on ATP cellular content in H4 and HeLa
469 cells (Fig. 10a). Similar to the well-known effect of mammalian SIRT3, SIRT8-3myc
470 expression increased ATP cellular content, suggesting that it shares with SIRT3 the ability
471 to enhance the activity of the mitochondrial ETC. Because an enhancement in the activity
472 of ETC can cause an increase in reactive oxygen species (ROS), we also evaluated the
473 levels of ROS in cells expressing SIRT8-3myc (Fig. 10b). We found similar ROS levels in
474 cells expressing SIRT3-like-3myc and untransfected cells (Fig. 10b). This finding
475 suggests that SIRT8 proteins share the mammalian SIRT3 characteristic of protection
476 against oxidative damage (Bause and Haigis 2013), likely by deacetylation of enzymes
477 involved in ROS clearance to protect mitochondrial membranes from oxidative stress
478 (Tseng et al. 2013). A candidate that could be activated by the deacetylation activity of
479 SIRT3-like proteins is SOD2 that in human cells reduces cellular ROS content promoting
480 oxidative stress resistance (Qiu et al. 2010; Tao et al. 2010). Alternatively, SIRT8 proteins
481 could activate the last complex of the ETC by deacetylation, enhancing ATP-synthase
482 activity without affecting ROS production, similar to the effect that SIRT3 has in response
483 to exercise-induced stress (Vassilopoulos et al. 2014). Together, our results show that
484 the SIRT8 protein is a new sirtuin family member with deacetylase activity that could have
485 important roles in the homeostasis of oxidative species and mitochondrial metabolism.

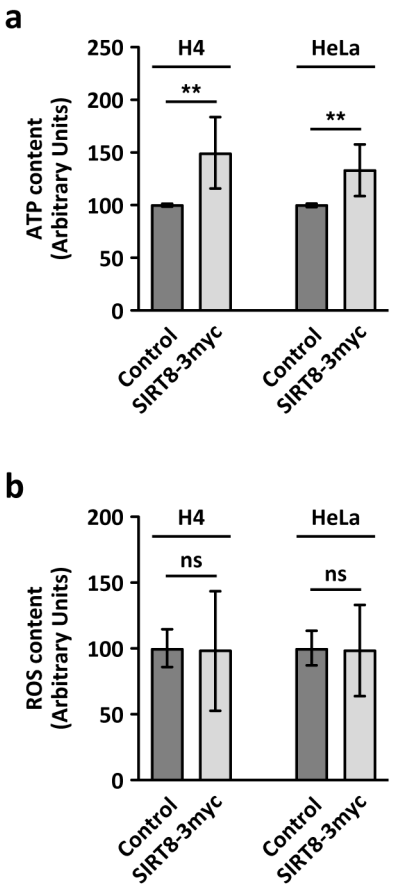

Figure 10. SIRT8-3myc expression causes an increment on ATP cellular content with no difference in ROS levels. (a) ATP levels were measured by a luciferin/luciferase bioluminescence assay in H4 and HeLa cells either left untreated (Control) or transiently expressing SIRT8-3myc. (b) ROS content was measured by the intensity fluorescence of the dye CM-H2DCFDA in H4 and HeLa cells either left untreated (Control) or transiently expressing SIRT8-3myc. Bars represent the mean ± standard deviation. Statistical analysis was performed using two-tailed unpaired Student's t-test (n = 4; ** $p < 0.01$; ns, not statistically significant).

Conclusions

We performed an evolutionary analysis of the sirtuin gene family in vertebrates. In addition to describing the duplicative history of sirtuins, our phylogenetic analyses revealed the presence of a new gene family member, *SIRT8*. This new vertebrate gene lineage is present in all vertebrates other than mammals, birds, and reptiles. Furthermore, our transcriptomic analyses show that *SIRT8* is transcribed in almost all examined tissues, showing a tendency to be more expressed in the ovary, suggesting biological

503 functions related to reproduction. According to our analyses, SIRT8 localized in the
504 mitochondria, had deacetylase activity and increased the ATP cellular content. The
505 finding of a new sirtuin gene lineage highlights the need for more detailed assessments
506 of orthology with a more broad taxonomic sampling to better define the membership
507 composition of gene families (Glover et al. 2019). In the literature, there are examples in
508 which more comprehensive analyses provide a better description of gene families,
509 including previously unknown family members (Castro et al. 2012; Wichmann et al. 2016;
510 Céspedes et al. 2017; Ramos-Vicente et al. 2018; Opazo, Kuraku, et al. 2019; Opazo,
511 Hoffmann, et al. 2019). The availability of species with different gene repertoires could be
512 seen as a natural experiment (Albertson et al. 2009) that helps us understand the
513 evolutionary fate of duplicated genes, as they can fulfill the biological functions associated
514 with the gene family but with a different combination of paralogs.
515

516 **Methods**

517 Protein sequences and phylogenetic analyses

518 We retrieved sirtuin amino acid sequences in representative species of all main groups
519 of vertebrates. Our sampling included mammals, birds, reptiles, amphibians, lungfish,
520 coelacanth, bony fish, cartilaginous fish, and cyclostomes (Supplementary Table S1).
521 Sequences were obtained from the Orthologous MAtrix project (OMA), December 2021
522 release (Altenhoff et al. 2021)last accessed on April 8th, 2022). In addition, we
523 complemented our sampling by retrieving sequences from vertebrate groups that were
524 not present or poorly represented in the Orthologous MAtrix project (e.g., crocodiles) from
525 the National Center for Biotechnology Information (NCBI) (Sharma et al. 2019) using the
526 program blast (tblastn) with default parameters (Altschul et al. 1990) Supplementary
527 Table S1). Protein sequences were aligned using the software MAFFT v.7 (Katoh and
528 Standley 2013), allowing the program to choose the alignment strategy (FFT-NS-i,
529 alignment length 2490 amino acids). To select the best-fitting model of molecular
530 evolution we used the proposed model tool in the program IQ-Tree v1.6.12
531 (Kalyaanamoorthy et al. 2017), which selected JTT+F+I+G4. We used a maximum-
532 likelihood approach to obtain the best tree using the program IQ-Tree v1.6.12
533 (Trifinopoulos et al. 2016). We carried out 20 independent runs to explore the tree space

534 changing the value of the strength of the perturbation (-pers) parameter. We conducted
535 the following analyses:
536 1. Five runs modifying the strength of the perturbation parameter from 0.5 (default
537 value) to 0.3.
538 2. Five runs using the default value (0.5) for the strength of the perturbation
539 parameter.
540 3. Five runs modifying the strength of the perturbation parameter from 0.5 (default
541 value) to 0.7.
542 4. Five runs modifying the strength of the perturbation parameter from 0.5 (default
543 value) to 0.9.
544 In all cases, the number of unsuccessful iterations to stop parameter (-nstop) value was
545 changed from 100 (default value) to 500. The tree with the highest likelihood score was
546 chosen (log-likelihood: -127052.963, -pers 0.5 and -nstop 500). Support for the nodes
547 was evaluated using two approaches: the aBayes test (Anisimova et al. 2011) and the
548 ultrafast bootstrap procedure using 1000 replicates (Hoang et al. 2018). Nicotinamide
549 Nucleotide Transhydrogenase (NNT) protein sequences, a member of the DHS-like
550 NAD/FAD-binding domain superfamily, from the human (*Homo sapiens*), mouse (*Mus*
551 *musculus*), zebrafish (*Danio rerio*) and spotted gar (*Lepisosteus oculatus*) were used as
552 outgroups.
553

554 ## Assessment of conserved synteny

555 We examined genes found upstream and downstream of the sirtuin genes. For
556 comparative purposes, we used the estimates of orthology and paralogy derived from the
557 Ensembl Compara database (Herrero et al. 2016); these estimates are obtained from a
558 pipeline that considers both synteny and phylogeny to generate orthology mappings.
559 These predictions were visualized using the program Genomicus v100.01 (Nguyen et al.
560 2018). Our assessments were performed in humans (*Homo sapiens*), chicken (*Gallus*
561 *gallus*), gharial (*Gavialis gangeticus*), red-eared slider (*Trachemys scripta*), green anole
562 (*Anolis carolinensis*), tropical clawed frog (*Xenopus tropicalis*), coelacanth (*Latimeria*
563 *chalumnae*), spotted gar (*Lepisosteus oculatus*), and elephant shark (*Callorhinchus milii*).
564

565 ## Dot-plots

566 We retrieved the chromosomal region containing the *SIRT8* gene of the tropical clawed
567 frog (*Xenopus tropicalis*, Ch3) including 6.7 kb up- and downstream, and the
568 corresponding syntenic region in the human (*Homo sapiens*, Chr12), opossum
569 (*Monodelphis domestica*, Chr8), chicken (*Gallus gallus*, Chr1), gharial (*Gavialis*
570 *gangeticus*, NW_017729022.1), red-eared slider (*Trachemys scripta*, Chr1), and green
571 anole (*Anolis carolinensis*, Chr5) based on the location of the flanking genes (*RIC8B* and
572 *TMEM263*). We aligned SIRT3-like syntenic regions using Advanced PipMaker (Schwartz
573 et al. 2000).

574

575 ## Transcript abundance analyses

576 Sirtuin transcript abundance was measured from a representative sample of vertebrates
577 including the elephant shark (*Callorhinchus milii*), zebrafish (*Danio rerio*), tropical clawed
578 frog (*Xenopus tropicalis*), anole lizard (*Anolis carolinensis*), and human (*Homo sapiens*).
579 RNASeq libraries from brain, heart, kidney, liver, muscle, ovary, and testis from each
580 species were gathered from the NCBI Short Read Archive (SRA; (Leinonen et al. 2011).
581 Accession numbers for species and tissue specific libraries can be found in Supplemental
582 Table S2. Reference transcript sequences were collected from Ensembl v.100 (Yates et
583 al. 2020) and we removed sequences that were shorter than 100 bp. For each library
584 adapters were removed using Trimmomatic 0.38 (Bolger et al. 2014) and reads were
585 filtered for quality using the parameters HEADCROP:5, SLIDINGWINDOW:5:30, and
586 MINLEN:50. We mapped quality filtered paired-end RNAseq reads back to reference
587 sequences using Bowtie 1.2.2 (Langmead et al. 2009) and default parameters of RSEM
588 (Li and Dewey 2011). Transcripts with < 10 mapped reads across all seven tissues per
589 species were removed prior to normalization. Normalization of raw read counts for each
590 species was performed using the median of ratios (Anders and Huber 2010) method
591 implemented by the estimateSizeFactors function in DESeq2 v1.26 (Love et al. 2014).
592 Briefly, for all samples within a species, the geometric mean is calculated for the read
593 counts of each gene. Read counts are then divided by the geometric mean and the
594 median ratio is determined for each sample. Normalized read counts are calculated by
595 dividing raw read counts by the sample-specific median ratio. If multiple SIRT transcripts

596 were present, we presented the expression data from the transcript with the most mapped
597 reads.
598

599 Protein structure homology modeling

600 Protein structure homology modeling was performed using the SWISS-MODEL server
601 (https://swissmodel.expasy.org/) (Waterhouse et al. 2018). Structural figures were
602 prepared with PyMOL Molecular Graphics System, Version 2.0.6 Schrödinger, LLC.
603

604 Recombinant cDNA Constructs

605 For expression in mammalian cells, a codon-optimized mammalian expression construct
606 encoding full-length (amino acids 1-372) elephant shark (*Callorhinchus milii*) SIRT8
607 (Supplementary table S1), cloned in-frame into the *Eco*RI and *Sal*I sites of the pCMV-
608 3Tag-4a vector followed by vector encoding sequence of three successive Myc epitope
609 tags before a stop codon, was acquired from GenScript (Piscataway, NJ). For the
610 generation of a codon-optimized bacterial expression construct, a cDNA encoding N-
611 terminal truncated (amino acids 95-372) elephant shark SIRT8, cloned in-frame into the
612 *Eco*RI and *Sal*I sites of the pGEX-4T-1 vector, was also acquired from GenScript. This
613 cDNA was subsequently cloned in-frame into the *Eco*RI and *Sal*I sites of the pGST-
614 Parallel-1 vector (Sheffield et al. 1999). The nucleotide sequence of all recombinant
615 constructs was confirmed by dideoxy sequencing using the AUSTRAL-omics core facility
616 at Universidad Austral de Chile (https://australomics.cl/).
617

618 Cell culture, cell transfection and preparation of protein extracts

619 H4 human neuroglioma cells, HeLa human cervix adenocarcinoma cells and MDA-MB-
620 231 human mammary gland adenocarcinoma cells were obtained from the American
621 Type Culture Collection (Manassas, VA). H4 and HeLa cells were maintained in
622 Dulbecco's modified Eagle's medium (DMEM), and MDA-MB-231 in DMEM-F12
623 (ThermoFisher, Waltham, MA). For all cell lines, media were supplemented with 10%
624 heat-inactivated fetal bovine serum, 100 U/ml penicillin, 100 µg/ml streptomycin
625 (ThermoFisher), and 5 µg/ml plasmocin (InvivoGen, San Diego, CA), and cells were
626 cultured in a humidified incubator with 5% CO_2 at 37 °C. For transient transfections, cells

627 were either seeded on top of glass coverslips on 24-well plates or on 6-well plates. When
628 cells were ~60% confluent, transfections were performed with Lipofectamine 2000
629 (ThermoFisher), according to the manufacturer's instructions. Preparation of protein
630 extracts from cultured, transfected or non-transfected cells was performed using methods
631 described elsewhere (Tenorio et al. 2016).
632

633 ## Antibodies and cell reagents

634 We used the following antibodies: mouse clone 9E10 against the c-Myc epitope
635 (Covance, Princeton, NJ), mouse clone BA3R against β-ACTIN (ThermoFisher), rabbit
636 polyclonal against Cytoskeleton-associated protein 4 (P63; Merck, Germany; cat #
637 HPA001225), and sheep polyclonal against Trans-Golgi network integral membrane
638 protein 2 (TGN46; Bio-Rad Laboratories, Hercules, CA; cat # AHP500G). The following
639 fluorochrome-conjugated antibodies were from ThermoFisher: Alexa Fluor-488–
640 conjugated donkey anti mouse IgG, Alexa Fluor-594–conjugated donkey anti rabbit IgG
641 and Alexa Fluor-647-conjugated donkey anti sheep IgG. HRP-conjugated secondary
642 antibodies were from Jackson ImmunoResearch (West Grove, PA). Depending on their
643 reactivity, primary antibodies were used at a dilution 1/200 to 1/2000. HRP-conjugated
644 secondary antibodies were used at dilutions 1/5000 to 1/20000 also depending on their
645 reactivity. All Alexa Fluor-conjugated secondary antibodies were used at a dilution
646 1/1000. The fluorescent nuclear stain 4',6-diamidino-2-phenylindole (DAPI) was also from
647 ThermoFisher.
648

649 ## Protein Electrophoresis, Immunoblotting and Immunofluorescence
650 Microscopy

651 SDS-PAGE and immunoblotting were performed as described (Bustamante et al. 2020).
652 For fluorescence microscopy, cells grown on glass coverslips were transfected, and after
653 16-h cells were left untreated or treated for 30 min with MitoTracker™ Orange CMTMRos
654 (ThermoFisher) according to the manufacturer's instructions. After washing with
655 phosphate buffered saline (PBS) supplemented with 0.1 mM $CaCl_2$ and 1 mM $MgCl_2$
656 (PBS-CM), cells were fixed in 4% paraformaldehyde for 30 min at room temperature,
657 permeabilized with 0.2% Triton X-100 in PBS-CM for 15 min at room temperature, and

658 incubated with blocking solution (0.2% gelatin in PBS-CM) for 10 min at room
659 temperature. Cells were incubated simultaneously either with antibodies to the c-Myc
660 epitope (1/200) and to TGN46 (1/1000) or to the c-Myc epitope, to TGN46 and to P63
661 (1/600) for 30 min at 37 ºC in a humidified chamber. After washing coverslips with PBS,
662 cells were incubated as before, but with fluorochrome-conjugated antibodies, followed by
663 PBS-washing, and coverslips were mounted onto glass slides with Fluoromount-G
664 mounting medium (ThermoFisher). Fluorescence microscopy images were acquired with
665 an AxioObserver.D1 microscope equipped with a PlanApo 63x oil immersion objective
666 (NA 1.4), and an AxioCam MRm digital camera (Carl Zeiss). To quantitatively evaluate
667 colocalization of fluorescence signals, we obtained the Pearson's correlation coefficient
668 and cytofluorograms of pairwise comparisons from images acquired under identical
669 settings, avoiding signal saturation and corrected for background, crosstalk and noise
670 signals on each set of images, using the plugin JACoP (Bolte and Cordelières 2006)
671 implemented in the software ImageJ (version 1.47h)(Schneider et al. 2012), and the
672 plugin Colocalization Finder implemented in the software ImageJ2 (version 2.3.0/1.53)
673 (Rueden et al. 2017). To prepare figures, 12-bit images were processed with ImageJ
674 software and Adobe Photoshop CS3 software (Adobe Systems, Mountain View, CA).
675

676 Expression and Purification of Recombinant N-terminal truncated elephant 677 shark SIRT8 protein

678 Recombinant, N-terminal truncated elephant shark SIRT8 (**Δ**NT-SIRT8; amino acids 95-
679 372) tagged with an N-terminal glutathione S-transferase (GST) followed by a tobacco
680 etch virus (TEV) protease cleavage site was expressed and purified using a method
681 described previously (Ross et al. 2014), with some modifications. Briefly, expression in
682 *E. coli* B834(DE3) (Novagen, Madison, WI) was induced with 0.25 mM IPTG at 25 °C for
683 16 h. Pellets of bacteria were resuspended in homogenization buffer (50 mM Tris HCl,
684 0.5 M NaCl, 5 mM EDTA, 5 mM β-mercaptoethanol, and 2 mM phenylmethylsulfonyl
685 fluoride, pH 8.0) and lysed by sonication. The clarified supernatant was purified on
686 glutathione-Sepharose 4B (GE Healthcare). After removal of the GST moiety by TEV
687 cleavage, and sequential further passage through glutathione-Sepharose 4B and Ni-NTA
688 (QIAGEN) resins, **Δ**NT-SIRT8 was further purified on a Superdex 200 pg column (GE

689 Healthcare) equilibrated in storage buffer (50 mM Tris HCl, 150 mM NaCl, 1 mM DTT).
690 Aliquots of purified protein were kept at -80 ºC until use.
691

692 ## Deacetylation activity

693 To characterize deacetylation activity of recombinant, N-terminal truncated elephant
694 shark SIRT8 (ΔNT-SIRT8), we used a fluorometric SIRT3 activity assay kit (Abcam, cat
695 # ab156067; Cambridge, UK), according to the manufacturer's instructions. This assay
696 allows detection of a fluorescent signal upon deacetylation of an acetylated substrate
697 peptide for recombinant human SIRT3. The intensity of fluorescence was measured on a
698 fluorometric microplate reader (Varioskan Flash, ThermoFisher) with excitation set at 350
699 nm and emission detection set at 450 nm. To analyze the deacetylation activity of N-
700 terminal truncated elephant shark SIRT8 protein, first we determined its optimum
701 temperature that resulted to be ~24 ºC. Subsequent analyses were performed by
702 comparing the activity of N-terminal truncated elephant shark SIRT8 protein at 24 ºC to
703 that of human SIRT3, which is provided by the assay kit, at 37 ºC. K_m and V_{max} were
704 obtained by varying the concentration of the fluorogenic acetylated substrate peptide
705 provided by the assay kit. This assay was also used to determine the effect of
706 nicotinamide (NAM), quercetin (QUE) and resveratrol (REV; Sigma-Aldrich) on the
707 deacetylation activity of ΔNT-SIRT8.
708

709 ## ATP and ROS content

710 ATP levels were quantified in cell lysates using a luciferin/luciferase bioluminescence
711 assay (ATP determination kit, Molecular Probes cat # A22066, Thermo Fisher Scientific)
712 as previously described (Jara et al. 2018). Briefly, cells were lysed in HEPES buffer (125
713 mM NaCl, 25 mM NaF, 1 mM EDTA, 1 mM EGTA, 1% NP-40, 25 mM HEPES, pH 7.4)
714 supplemented with a protease inhibitor mixture (cat # 78429, Thermo Fisher Scientific)
715 and centrifuged at 12000 rpm using a refrigerated centrifuge (Eppendorf model 5424R)
716 for 15 min at 4 ºC. Proteins in the supernatant were quantified, and 10 µl of lysate were
717 used to determine ATP levels according to the kit manufacturer's instructions. The ATP
718 level in each sample was calculated using standard curves and normalized to the protein
719 concentration in each sample. ROS content was determined in cell lysates using 25 µM

720 CM-H2DCFDA (DCF; a fluorogenic indicator of ROS), as previously described (Jara et
721 al. 2018; Olesen et al. 2020). The intensity of fluorescence was measured on a
722 fluorescence plate reader (Biotek Synergy HT, Agilent, Santa Clara, CA) with excitation
723 set at 485 nm and emission detection set at 530 nm. Briefly, in a dark 96-well plate, 25
724 µg of cell lysate proteins were incubated with CM-H2DCFDA (DCF) dye with shaking for
725 5 min at room temperature, followed by determination of the fluorescence of each sample
726 that was subtracted by the fluorescence of the respective blank.
727

728 ## Statistical Analysis

729 In the case of the deacetylation, ATP content and ROS content assays, quantification
730 was performed from at least three independent experiments/measurements. Statistical
731 analysis was performed using Microsoft Excel for Mac 2011 (Microsoft Corporation).
732 When appropriate, results are represented in graphs depicting the mean ± standard
733 deviation. Statistical significance was determined by two-tailed, paired t-test. P-values >
734 0.05 or ≤ 0.05 were regarded as not statistically significant or statistically significant,
735 respectively. In the figures, P-values between 0.01 and 0.05 are indicated with one
736 asterisk, P-values between 0.001 and 0.01 are indicated with two asterisks, and P-values
737 less than 0.001 are indicated with three asterisks.
738

739 ## Data accessibility

740 Data and supplementary material are available online:
741

742 ## Acknowledgements

743 This work was supported by the Fondo Nacional de Desarrollo Científico y Tecnológico
744 from Chile (FONDECYT 1210471) and The Millennium Nucleus of Ion Channel-
745 Associated Diseases is a Millennium Nucleus of the Millennium Scientific Initiative,
746 National Agency of Research and Development (ANID, NCN19_168), Ministry of Science,
747 Technology, Knowledge and Innovation, Chile to JCO, Fondo Nacional de Desarrollo
748 Científico y Tecnológico from Chile (FONDECYT 1211481) to GAM, National Science

Foundation (EPS-0903787, DBI-1262901 and DEB-1354147) to F.G.H., Financiamiento Basal No. ANID/BASAL/ACE210009 to PVB and No. ANID/BASAL/FB210008 to PVB and CTR, Fondap-Ideal Grant N° 15150003 to LV-C, ANID-Millennium Science Initiative Program-Center ICM-ANID ICN2021_002 to LV-C, Fondo Nacional de Desarrollo Científico y Tecnológico from Chile (FONDECYT 1180957) to FJM, Vicerrectoría de Investigación, Desarrollo y Creación Artística, Universidad Austral de Chile to JCO, FJM, LVC, GAM. We thank Stefanie Teuber, John Quiroga and Rafael Burgos, Instituto de Farmacología y Morfofisiología, Facultad de Ciencias Veterinarias, Universidad Austral de Chile, for providing assistance in the use of the Varioskan Flash microplate reader; Hianara Bustamante, Instituto de Microbiología Clínica, Facultad de Medicina, Universidad Austral de Chile, for providing quercetin and resveratrol; Víctor Castro, Departamento de Biología, Facultad de Ciencias, Universidad de Chile, for providing NAD^+ and nicotinamide; and Gonzalo Astroza, and Andrés Rivera-Dictter for technical assistance.

Contributions

JCO and GAM designed the study. JCO, MWV, FGH, KZ, CM, CL, VC, FJM, PVB, CTR, GAM, collected and/or analyzed data. JCO, PVB and GAM wrote the manuscript. JCO, MWV, FGH, KZ, CM, CL, VC, LV-C, FJM, PVB, CTR and GAM, reviewed and edited the manuscript. All authors contributed to the article and approved the submitted version.

Ethics declarations

Conflict of interest disclosure

The authors declare they have no conflict of interest relating to the content of this article. Juan C. Opazo is a recommender for PCI Evol Biol and PCI Genomics.

Data availability

Data and supplementary material are available online at zenodo.org

780 **References**

781 Albalat R, Cañestro C. 2016. Evolution by gene loss. *Nat. Rev. Genet.* 17:379–391.

782 Albertson RC, Craig Albertson R, Cresko W, William Detrich H, Postlethwait JH. 2009.
783 Evolutionary mutant models for human disease. *Trends in Genetics* [Internet]
784 25:74–81. Available from: http://dx.doi.org/10.1016/j.tig.2008.11.006

785 Altenhoff AM, Train C-M, Gilbert KJ, Mediratta I, Mendes de Farias T, Moi D, Nevers Y,
786 Radoykova H-S, Rossier V, Warwick Vesztrocy A, et al. 2021. OMA orthology in
787 2021: website overhaul, conserved isoforms, ancestral gene order and more.
788 *Nucleic Acids Res.* 49:D373–D379.

789 Altschul SF, Gish W, Miller W, Myers EW, Lipman DJ. 1990. Basic local alignment
790 search tool. *J. Mol. Biol.* 215:403–410.

791 Anderson KA, Green MF, Huynh FK, Wagner GR, Hirschey MD. 2014. SnapShot:
792 Mammalian Sirtuins. *Cell* 159:956–956.e1.

793 Anders S, Huber W. 2010. Differential expression analysis for sequence count data.
794 *Genome Biol.* 11:R106.

795 Anisimova M, Gil M, Dufayard J-F, Dessimoz C, Gascuel O. 2011. Survey of branch
796 support methods demonstrates accuracy, power, and robustness of fast likelihood-
797 based approximation schemes. *Syst. Biol.* 60:685–699.

798 Bause AS, Haigis MC. 2013. SIRT3 regulation of mitochondrial oxidative stress. *Exp.*
799 *Gerontol.* 48:634–639.

800 Bilyk KT, Zhuang X, Vargas-Chacoff L, Cheng C-HC. 2021. Evolution of chaperome
801 gene expression and regulatory elements in the antarctic notothenioid fishes.
802 *Heredity* 126:424–441.

803 Blander G, Guarente L. 2004. The Sir2 family of protein deacetylases. *Annu. Rev.*
804 *Biochem.* 73:417–435.

805 Bolger AM, Lohse M, Usadel B. 2014. Trimmomatic: a flexible trimmer for Illumina
806 sequence data. *Bioinformatics* 30:2114–2120.

807 Bolte S, Cordelières FP. 2006. A guided tour into subcellular colocalization analysis in
808 light microscopy. *J. Microsc.* 224:213–232.

809 Brown K, Xie S, Qiu X, Mohrin M, Shin J, Liu Y, Zhang D, Scadden DT, Chen D. 2013.
810 SIRT3 reverses aging-associated degeneration. *Cell Rep.* 3:319–327.

811 Bustamante HA, Cereceda K, González AE, Valenzuela GE, Cheuquemilla Y,
812 Hernández S, Arias-Muñoz E, Cerda-Troncoso C, Bandau S, Soza A, et al. 2020.
813 The Proteasomal Deubiquitinating Enzyme PSMD14 Regulates Macroautophagy

814 by Controlling Golgi-to-ER Retrograde Transport. *Cells* [Internet] 9. Available from:
815 http://dx.doi.org/10.3390/cells9030777

816 Castro LFC, Lopes-Marques M, Gonçalves O, Wilson JM. 2012. The evolution of
817 pepsinogen C genes in vertebrates: duplication, loss and functional diversification.
818 *PLoS One* 7:e32852.

819 Céspedes HA, Zavala K, Vandewege MW, Opazo JC. 2017. Evolution of the α-
820 adrenoreceptors in vertebrates: ADRA2D is absent in mammals and crocodiles.
821 *Gen. Comp. Endocrinol.* 250:85–94.

822 Costantini S, Sharma A, Raucci R, Costantini M, Autiero I, Colonna G. 2013. Genealogy
823 of an ancient protein family: the Sirtuins, a family of disordered members. *BMC*
824 *Evol. Biol.* 13:60.

825 Delsuc F, Brinkmann H, Chourrout D, Philippe H. 2006. Tunicates and not
826 cephalochordates are the closest living relatives of vertebrates. *Nature* 439:965–
827 968.

828 Delsuc F, Tsagkogeorga G, Lartillot N, Philippe H. 2008. Additional molecular support
829 for the new chordate phylogeny. *Genesis* 46:592–604.

830 Di Emidio G, Falone S, Artini PG, Amicarelli F, D'Alessandro AM, Tatone C. 2021.
831 Mitochondrial Sirtuins in Reproduction. *Antioxidants (Basel)* [Internet] 10. Available
832 from: http://dx.doi.org/10.3390/antiox10071047

833 Félix M-A, Barkoulas M. 2015. Pervasive robustness in biological systems. *Nat. Rev.*
834 *Genet.* 16:483–496.

835 Frye RA. 2000. Phylogenetic classification of prokaryotic and eukaryotic Sir2-like
836 proteins. *Biochem. Biophys. Res. Commun.* 273:793–798.

837 Frye RA. 2006. Evolution of Sirtuins From Archaea to Vertebrates. *Histone*
838 *Deacetylases* [Internet]:183–202. Available from: http://dx.doi.org/10.1385/1-59745-
839 024-3:183

840 Fujita Y, Yamashita T. 2018. Sirtuins in Neuroendocrine Regulation and Neurological
841 Diseases. *Front. Neurosci.* 12:778.

842 Gitelman I. 2007. Evolution of the vertebrate twist family and synfunctionalization: a
843 mechanism for differential gene loss through merging of expression domains. *Mol.*
844 *Biol. Evol.* 24:1912–1925.

845 Glover N, Dessimoz C, Ebersberger I, Forslund SK, Gabaldón T, Huerta-Cepas J,
846 Martin M-J, Muffato M, Patricio M, Pereira C, et al. 2019. Advances and
847 Applications in the Quest for Orthologs. *Mol. Biol. Evol.* 36:2157–2164.

848 Glozak MA, Sengupta N, Zhang X, Seto E. 2005. Acetylation and deacetylation of non-

histone proteins. *Gene* 363:15–23.

Goldberg T, Hecht M, Hamp T, Karl T, Yachdav G, Ahmed N, Altermann U, Angerer P, Ansorge S, Balasz K, et al. 2014. LocTree3 prediction of localization. *Nucleic Acids Res.* 42:W350–W355.

Greiss S, Gartner A. 2009. Sirtuin/Sir2 phylogeny, evolutionary considerations and structural conservation. *Mol. Cells* 28:407–415.

Haigis MC, Mostoslavsky R, Haigis KM, Fahie K, Christodoulou DC, Murphy AJ, Valenzuela DM, Yancopoulos GD, Karow M, Blander G, et al. 2006. SIRT4 inhibits glutamate dehydrogenase and opposes the effects of calorie restriction in pancreatic beta cells. *Cell* 126:941–954.

Haigis MC, Sinclair DA. 2010. Mammalian sirtuins: biological insights and disease relevance. *Annu. Rev. Pathol.* 5:253–295.

Hara Y, Yamaguchi K, Onimaru K, Kadota M, Koyanagi M, Keeley SD, Tatsumi K, Tanaka K, Motone F, Kageyama Y, et al. 2018. Shark genomes provide insights into elasmobranch evolution and the origin of vertebrates. *Nat Ecol Evol* 2:1761–1771.

Helsen J, Voordeckers K, Vanderwaeren L, Santermans T, Tsontaki M, Verstrepen KJ, Jelier R. 2020. Gene Loss Predictably Drives Evolutionary Adaptation. *Mol. Biol. Evol.* 37:2989–3002.

Herrero J, Muffato M, Beal K, Fitzgerald S, Gordon L, Pignatelli M, Vilella AJ, Searle SMJ, Amode R, Brent S, et al. 2016. Ensembl comparative genomics resources. *Database* [Internet] 2016. Available from: http://dx.doi.org/10.1093/database/bav096

Himmel NJ, Gray TR, Cox DN. 2020. Phylogenetics Identifies Two Eumetazoan TRPM Clades and an Eighth TRP Family, TRP Soromelastatin (TRPS). *Mol. Biol. Evol.* 37:2034–2044.

Hirschey MD. 2011. Old enzymes, new tricks: sirtuins are NAD(+)-dependent de-acylases. *Cell Metab.* 14:718–719.

Hirschey MD, Shimazu T, Goetzman E, Jing E, Schwer B, Lombard DB, Grueter CA, Harris C, Biddinger S, Ilkayeva OR, et al. 2010. SIRT3 regulates mitochondrial fatty-acid oxidation by reversible enzyme deacetylation. *Nature* 464:121–125.

Hoang DT, Chernomor O, von Haeseler A, Minh BQ, Vinh LS. 2018. UFBoot2: Improving the Ultrafast Bootstrap Approximation. *Mol. Biol. Evol.* 35:518–522.

Howe KL, Achuthan P, Allen J, Allen J, Alvarez-Jarreta J, Amode MR, Armean IM, Azov AG, Bennett R, Bhai J, et al. 2021. Ensembl 2021. *Nucleic Acids Res.* 49:D884–D891.

885 Iwabe N, Hara Y, Kumazawa Y, Shibamoto K, Saito Y, Miyata T, Katoh K. 2005. Sister
886 group relationship of turtles to the bird-crocodilian clade revealed by nuclear DNA-
887 coded proteins. *Mol. Biol. Evol.* 22:810–813.

888 Jara C, Aránguiz A, Cerpa W, Tapia-Rojas C, Quintanilla RA. 2018. Genetic ablation of
889 tau improves mitochondrial function and cognitive abilities in the hippocampus.
890 *Redox Biol* 18:279–294.

891 Kabiljo J, Murko C, Pusch O, Zupkovitz G. 2019. Spatio-temporal expression profile of
892 sirtuins during aging of the annual fish Nothobranchius furzeri. *Gene Expression*
893 *Patterns* [Internet] 33:11–19. Available from:
894 http://dx.doi.org/10.1016/j.gep.2019.05.001

895 Kalyaanamoorthy S, Minh BQ, Wong TKF, von Haeseler A, Jermiin LS. 2017.
896 ModelFinder: fast model selection for accurate phylogenetic estimates. *Nat.*
897 *Methods* 14:587–589.

898 Katoh K, Standley DM. 2013. MAFFT multiple sequence alignment software version 7:
899 improvements in performance and usability. *Mol. Biol. Evol.* 30:772–780.

900 Kumar S, Stecher G, Suleski M, Hedges SB. 2017. TimeTree: A Resource for
901 Timelines, Timetrees, and Divergence Times. *Mol. Biol. Evol.* 34:1812–1819.

902 Kuraku S. 2013. Impact of asymmetric gene repertoire between cyclostomes and
903 gnathostomes. *Semin. Cell Dev. Biol.* 24:119–127.

904 Langmead B, Trapnell C, Pop M, Salzberg SL. 2009. Ultrafast and memory-efficient
905 alignment of short DNA sequences to the human genome. *Genome Biol.* 10:R25.

906 Leinonen R, Sugawara H, Shumway M, International Nucleotide Sequence Database
907 Collaboration. 2011. The sequence read archive. *Nucleic Acids Res.* 39:D19–D21.

908 Li B, Dewey CN. 2011. RSEM: accurate transcript quantification from RNA-Seq data
909 with or without a reference genome. *BMC Bioinformatics* [Internet] 12. Available
910 from: http://dx.doi.org/10.1186/1471-2105-12-323

911 Love MI, Huber W, Anders S. 2014. Moderated estimation of fold change and
912 dispersion for RNA-seq data with DESeq2. *Genome Biol.* 15:550.

913 Lynch M, Conery JS. 2000. The Evolutionary Fate and Consequences of Duplicate
914 Genes. *Science* [Internet] 290:1151–1155. Available from:
915 http://dx.doi.org/10.1126/science.290.5494.1151

916 McBurney MW, Yang X, Jardine K, Hixon M, Boekelheide K, Webb JR, Lansdorp PM,
917 Lemieux M. 2003. The mammalian SIR2alpha protein has a role in embryogenesis
918 and gametogenesis. *Mol. Cell. Biol.* 23:38–54.

919 McCormick SD. 1993. Methods for nonlethal gill biopsy and measurement of Na+, K+-

920 ATPase activity. *Can. J. Fish. Aquat. Sci.* 50:656–658.

921 McDonnell E, Peterson BS, Bomze HM, Hirschey MD. 2015. SIRT3 regulates
922 progression and development of diseases of aging. *Trends Endocrinol. Metab.*
923 26:486–492.

924 Michan S, Sinclair D. 2007. Sirtuins in mammals: insights into their biological function.
925 *Biochem. J* 404:1–13.

926 Michishita E, Park JY, Burneskis JM, Barrett JC, Horikawa I. 2005. Evolutionarily
927 conserved and nonconserved cellular localizations and functions of human SIRT
928 proteins. *Mol. Biol. Cell* 16:4623–4635.

929 Nei M, Rooney AP. 2005. Concerted and birth-and-death evolution of multigene
930 families. *Annu. Rev. Genet.* 39:121–152.

931 Nguyen NTT, Vincens P, Roest Crollius H, Louis A. 2018. Genomicus 2018: karyotype
932 evolutionary trees and on-the-fly synteny computing. *Nucleic Acids Res.* 46:D816–
933 D822.

934 North BJ, Verdin E. 2004. Sirtuins: Sir2-related NAD-dependent protein deacetylases.
935 *Genome Biol.* 5:224.

936 Ohno S. 1985. Dispensable genes. *Trends Genet.* 1:160–164.

937 Olesen MA, Torres AK, Jara C, Murphy MP, Tapia-Rojas C. 2020. Premature synaptic
938 mitochondrial dysfunction in the hippocampus during aging contributes to memory
939 loss. *Redox Biol* 34:101558.

940 Olson MV. 1999. When less is more: gene loss as an engine of evolutionary change.
941 *Am. J. Hum. Genet.* 64:18–23.

942 Onyango P, Celic I, McCaffery JM, Boeke JD, Feinberg AP. 2002. SIRT3, a human
943 SIR2 homologue, is an NAD-dependent deacetylase localized to mitochondria.
944 *Proc. Natl. Acad. Sci. U. S. A.* 99:13653–13658.

945 Opazo JC, Hoffmann FG, Zavala K, Edwards SV. 2019. Evolution of the DAN gene
946 family in vertebrates. *Evolutionary Biology*:185.

947 Opazo JC, Kuraku S, Zavala K, Toloza-Villalobos J, Hoffmann FG. 2019. Evolution of
948 nodal and nodal-related genes and the putative composition of the heterodimers
949 that trigger the nodal pathway in vertebrates. *Evolution & Development* [Internet]
950 21:205–217. Available from: http://dx.doi.org/10.1111/ede.12292

951 Opazo JC, Vandewege MW, Gutierrez J, Zavala K, Vargas-Chacoff L, Morera FJ,
952 Mardones GA. 2021. Independent duplications of the Golgi phosphoprotein 3
953 oncogene in birds. *Sci. Rep.* 11:12483.

954 Pereira TCB, Rico EP, Rosemberg DB, Schirmer H, Dias RD, Souto AA, Bonan CD,
955 Bogo MR. 2011. Zebrafish as a model organism to evaluate drugs potentially able
956 to modulate sirtuin expression. *Zebrafish* 8:9–16.

957 Ponnambalam S, Girotti M, Yaspo ML, Owen CE, Perry AC, Suganuma T, Nilsson T,
958 Fried M, Banting G, Warren G. 1996. Primate homologues of rat TGN38: primary
959 structure, expression and functional implications. *J. Cell Sci.* 109 (Pt 3):675–685.

960 Qiu H, Hildebrand F, Kuraku S, Meyer A. 2011. Unresolved orthology and peculiar
961 coding sequence properties of lamprey genes: the KCNA gene family as test case.
962 *BMC Genomics* 12:325.

963 Qiu X, Brown K, Hirschey MD, Verdin E, Chen D. 2010. Calorie restriction reduces
964 oxidative stress by SIRT3-mediated SOD2 activation. *Cell Metab.* 12:662–667.

965 Rajabi N, Galleano I, Madsen AS, Olsen CA. 2018. Targeting Sirtuins: Substrate
966 Specificity and Inhibitor Design. *Prog. Mol. Biol. Transl. Sci.* 154:25–69.

967 Ramos-Vicente D, Ji J, Gratacòs-Batlle E, Gou G, Reig-Viader R, Luís J, Burguera D,
968 Navas-Perez E, García-Fernández J, Fuentes-Prior P, et al. 2018. Metazoan
969 evolution of glutamate receptors reveals unreported phylogenetic groups and
970 divergent lineage-specific events. *Elife* [Internet] 7. Available from:
971 http://dx.doi.org/10.7554/eLife.35774

972 Ross BH, Lin Y, Corales EA, Burgos PV, Mardones GA. 2014. Structural and functional
973 characterization of cargo-binding sites on the μ4-subunit of adaptor protein complex
974 4. *PLoS One* 9:e88147.

975 Rueden CT, Schindelin J, Hiner MC, DeZonia BE, Walter AE, Arena ET, Eliceiri KW.
976 2017. ImageJ2: ImageJ for the next generation of scientific image data. *BMC*
977 *Bioinformatics* 18:529.

978 Saravia J, Paschke K, Oyarzún-Salazar R, Cheng C-HC, Navarro JM, Vargas-Chacoff
979 L. 2021. Effects of warming rates on physiological and molecular components of
980 response to CTMax heat stress in the Antarctic fish Harpagifer antarcticus. *J.*
981 *Therm. Biol.* 99:103021.

982 Sauve AA, Schramm VL. 2003. Sir2 regulation by nicotinamide results from switching
983 between base exchange and deacetylation chemistry. *Biochemistry* 42:9249–9256.

984 Scher MB, Vaquero A, Reinberg D. 2007. SirT3 is a nuclear NAD+-dependent histone
985 deacetylase that translocates to the mitochondria upon cellular stress. *Genes Dev.*
986 21:920–928.

987 Schneider CA, Rasband WS, Eliceiri KW. 2012. NIH Image to ImageJ: 25 years of
988 image analysis. *Nat. Methods* 9:671–675.

989 Scholte LLS, Mourão MM, Pais FS-M, Melesina J, Robaa D, Volpini AC, Sippl W, Pierce

990 RJ, Oliveira G, Nahum LA. 2017. Evolutionary relationships among protein lysine
991 deacetylases of parasites causing neglected diseases. *Infect. Genet. Evol.* 53:175–
992 188.

993 Schwartz S, Zhang Z, Frazer KA, Smit A, Riemer C, Bouck J, Gibbs R, Hardison R,
994 Miller W. 2000. PipMaker--a web server for aligning two genomic DNA sequences.
995 *Genome Res.* 10:577–586.

996 Schweizer A, Ericsson M, Bächi T, Griffiths G, Hauri HP. 1993. Characterization of a
997 novel 63 kDa membrane protein. Implications for the organization of the ER-to-
998 Golgi pathway. *J. Cell Sci.* 104 (Pt 3):671–683.

999 Schwer B, North BJ, Frye RA, Ott M, Verdin E. 2002. The human silent information
1000 regulator (Sir)2 homologue hSIRT3 is a mitochondrial nicotinamide adenine
1001 dinucleotide-dependent deacetylase. *J. Cell Biol.* 158:647–657.

1002 Shahgaldi S, Kahmini FR. 2021. A comprehensive review of Sirtuins: With a major focus
1003 on redox homeostasis and metabolism. *Life Sci.* 282:119803.

1004 Sharma S, Ciufo S, Starchenko E, Darji D, Chlumsky L, Karsch-Mizrachi I, Schoch CL.
1005 2019. The NCBI BioCollections Database. *Database* [Internet] 2019. Available
1006 from: http://dx.doi.org/10.1093/database/baz057

1007 Sheffield P, Garrard S, Derewenda Z. 1999. Overcoming expression and purification
1008 problems of RhoGDI using a family of “parallel” expression vectors. *Protein Expr.*
1009 *Purif.* 15:34–39.

1010 Simó-Mirabet P, Bermejo-Nogales A, Calduch-Giner JA, Pérez-Sánchez J. 2017.
1011 Tissue-specific gene expression and fasting regulation of sirtuin family in gilthead
1012 sea bream (Sparus aurata). *Journal of Comparative Physiology B* [Internet]
1013 187:153–163. Available from: http://dx.doi.org/10.1007/s00360-016-1014-0

1014 Slade KM, Freggiaro S, Cottrell KA, Smith JJ, Wiley EA. 2011. Sirtuin-mediated nuclear
1015 differentiation and programmed degradation in Tetrahymena. *BMC Cell Biol.* 12:40.

1016 Smith JJ, Kuraku S, Holt C, Sauka-Spengler T, Jiang N, Campbell MS, Yandell MD,
1017 Manousaki T, Meyer A, Bloom OE, et al. 2013. Sequencing of the sea lamprey
1018 (Petromyzon marinus) genome provides insights into vertebrate evolution. *Nat.*
1019 *Genet.* 45:415–421, 421e1–e2.

1020 Somero GN. 2004. Adaptation of enzymes to temperature: searching for basic
1021 “strategies.” *Comp. Biochem. Physiol. B Biochem. Mol. Biol.* 139:321–333.

1022 Stelzer G, Rosen N, Plaschkes I, Zimmerman S, Twik M, Fishilevich S, Stein TI, Nudel
1023 R, Lieder I, Mazor Y, et al. 2016. The GeneCards Suite: From Gene Data Mining to
1024 Disease Genome Sequence Analyses. *Curr. Protoc. Bioinformatics* 54:1.30.1–
1025 1.30.33.

1026 Tao R, Coleman MC, Pennington JD, Ozden O, Park S-H, Jiang H, Kim H-S, Flynn CR,
1027 Hill S, Hayes McDonald W, et al. 2010. Sirt3-mediated deacetylation of
1028 evolutionarily conserved lysine 122 regulates MnSOD activity in response to stress.
1029 *Mol. Cell* 40:893–904.

1030 Tatone C, Di Emidio G, Barbonetti A, Carta G, Luciano AM, Falone S, Amicarelli F.
1031 2018. Sirtuins in gamete biology and reproductive physiology: emerging roles and
1032 therapeutic potential in female and male infertility. *Hum. Reprod. Update* 24:267–
1033 289.

1034 Tenorio MJ, Ross BH, Luchsinger C, Rivera-Dictter A, Arriagada C, Acuña D, Aguilar M,
1035 Cavieres V, Burgos PV, Ehrenfeld P, et al. 2016. Distinct Biochemical Pools of
1036 Golgi Phosphoprotein 3 in the Human Breast Cancer Cell Lines MCF7 and MDA-
1037 MB-231. *PLoS One* 11:e0154719.

1038 Trifinopoulos J, Nguyen L-T, von Haeseler A, Minh BQ. 2016. W-IQ-TREE: a fast online
1039 phylogenetic tool for maximum likelihood analysis. *Nucleic Acids Res.* 44:W232–
1040 W235.

1041 Tseng AHH, Shieh S-S, Wang DL. 2013. SIRT3 deacetylates FOXO3 to protect
1042 mitochondria against oxidative damage. *Free Radic. Biol. Med.* 63:222–234.

1043 Vassilopoulos A, Fritz KS, Petersen DR, Gius D. 2011. The human sirtuin family:
1044 evolutionary divergences and functions. *Hum. Genomics* 5:485–496.

1045 Vassilopoulos A, Pennington JD, Andresson T, Rees DM, Bosley AD, Fearnley IM, Ham
1046 A, Flynn CR, Hill S, Rose KL, et al. 2014. SIRT3 deacetylates ATP synthase F1
1047 complex proteins in response to nutrient- and exercise-induced stress. *Antioxid.*
1048 *Redox Signal.* 21:551–564.

1049 Vazquez BN, Vaquero A, Schindler K. 2020. Sirtuins in female meiosis and in
1050 reproductive longevity. *Mol. Reprod. Dev.* 87:1175–1187.

1051 Waterhouse A, Bertoni M, Bienert S, Studer G, Tauriello G, Gumienny R, Heer FT, de
1052 Beer TAP, Rempfer C, Bordoli L, et al. 2018. SWISS-MODEL: homology modelling
1053 of protein structures and complexes. *Nucleic Acids Res.* 46:W296–W303.

1054 Wichmann IA, Zavala K, Hoffmann FG, Vandewege MW, Corvalán AH, Amigo JD,
1055 Owen GI, Opazo JC. 2016. Evolutionary history of the reprimo tumor suppressor
1056 gene family in vertebrates with a description of a new reprimo gene lineage. *Gene*
1057 591:245–254.

1058 Wood JG, Rogina B, Lavu S, Howitz K, Helfand SL, Tatar M, Sinclair D. 2004. Sirtuin
1059 activators mimic caloric restriction and delay ageing in metazoans. *Nature*
1060 430:686–689.

1061 Yang L, Ma X, He Y, Yuan C, Chen Q, Li G, Chen X. 2017. Sirtuin 5: a review of
1062 structure, known inhibitors and clues for developing new inhibitors. *Sci. China Life*

1063 *Sci.* 60:249–256.

1064 Yates AD, Achuthan P, Akanni W, Allen J, Allen J, Alvarez-Jarreta J, Amode MR,
1065 Armean IM, Azov AG, Bennett R, et al. 2020. Ensembl 2020. *Nucleic Acids Res.*
1066 48:D682–D688.

1067 You W, Zheng W, Weiss S, Chua KF, Steegborn C. 2019. Structural basis for the
1068 activation and inhibition of Sirtuin 6 by quercetin and its derivatives. *Sci. Rep.*
1069 9:19176.

1070 Zhang J, Xiang H, Liu J, Chen Y, He R-R, Liu B. 2020. Mitochondrial Sirtuin 3: New
1071 emerging biological function and therapeutic target. *Theranostics* 10:8315–8342.

1072 Zhao E, Hou J, Ke X, Abbas MN, Kausar S, Zhang L, Cui H. 2019. The Roles of Sirtuin
1073 Family Proteins in Cancer Progression. *Cancers* [Internet] 11. Available from:
1074 http://dx.doi.org/10.3390/cancers11121949

1075 Zhao H-C, Ding T, Ren Y, Li T-J, Li R, Fan Y, Yan J, Zhao Y, Li M, Yu Y, et al. 2016.
1076 Role of Sirt3 in mitochondrial biogenesis and developmental competence of human
1077 in vitro matured oocytes. *Hum. Reprod.* 31:607–622.